Contents lists available at ScienceDirect

Materials Today Energy

journal homepage: www.elsevier.com

Journal Cover Image

Carbon nanotube wools made directly from CO_2 by molten electrolysis: Value driven pathways to carbon dioxide greenhouse gas mitigation

Marcus Johnson, Jiawen Ren, Matthew Lefler, Gad Licht, Juan Vicini, Xinye Liu, Stuart Licht*

Dept. of Chemistry, George Washington University, Washington DC 20052, USA

ARTICLE INFO

Article history:
Received 25 June 2017
Received in revised form 4 July 2017
Accepted 9 July 2017
Available online xxx

ABSTRACT

A climate mitigation comprehensive solution is presented through the first high yield, low energy synthesis of macroscopic length carbon nanotube ("CNT") wool from CO_2 by molten carbonate electrolysis. The CNT wool is of length suitable for weaving into carbon composites and textiles. Growing CO_2 concentrations, and the concurrent climate change and species extinction, can be addressed if CO_2 becomes a sought resource rather than a greenhouse pollutant. Inexpensive carbon composites formed from carbon wool as a lighter metal, textiles or cement replacement comprise major market sinks to compactly store transformed anthropogenic CO_2. 100×-longer CNTs grow on Monel versus steel. Monel, electrolyte equilibration, and a mixed metal nucleation facilitate the synthesis. CO_2, the sole reactant in this transformation, is directly extractable from dilute (atmospheric) or concentrated sources, and the analyzed production cost of $660 per ton CNT is cost constrained only by the (low) cost of electricity. Today's market valuation of >$100,000 per ton CNT incentivizes CO_2 removal.

The first electrosynthesis of carbon nanotube wool is shown, and the only reactant, CO_2, becomes a useful, valuable resource rather than a greenhouse pollutant as a comprehensive response to removal of anthropogenic carbon dioxide.

1. Introduction

The first facile high yield, low energy synthesis of macroscopic length carbon nanotubes (CNTs) from CO_2 by molten carbonate electrolysis is demonstrated here. This CNT "wool" is of length and uniformity suitable for weaving into carbon composites and textiles, and presents an unusual and perhaps distinct new class of materials. CNT products have a contemporary market value in the $100 K per ton range [1]. Whereas our previous molten carbonate synthesized CNTs have nanometer-sized diameter and lengths, this CNT wool reaches diameters over 1 μm and length over 1 mm. Hence, the question arises whether this new CNT wool should be classified as a nanomaterial. The physical properties, such as the unusually high electrical conductivity and Raman spectra of these materials demonstrated in the linked Data in Brief paper are that of multiwalled carbon nanotubes, and are due to the morphology as demonstrated by TEM. The length to diameter ratio and the 0.342 nm inter-wall spacing of these confined cylindrical graphene layers suggests these new CNT wools should be classified as a (albeit unusual, but particularly useful as a cloth precursor, class of) CNT material. Monel cathode substrates, electrolyte equilibration, and a mixed metal (NiChrome) nucleation facilitate the synthesis of this CNT wool. The process is constrained by the (low) cost of electricity. *Carbon dioxide is the sole reactant in this CNT transformation*, providing a financial impetus for the removal of this greenhouse gas.

The planet is heating up. The atmospheric CO_2 concentration, which had cycled at 235 ± ~50 ppm for 400,000 years until 1850, is currently at 406–410 ppm and rising [2,3]. In l824 Fourier found that our atmosphere insulates the Earth; in 1864 Tyndall measured CO_2 infrared absorption heating up the Earth. The thermal interactive dynamics of the land/sea/air are complex, but by 1896 Nobel laureate Arrhenius (physicist, chemist, and electrolytic theory) estimated the greenhouse effect magnitude and wrote in 1908 in the Worlds in the Making: "any doubling of the percentage of carbon dioxide in the air would raise the temperature of the earth's surface by 4 °C; … The enormous combustion of coal by our industrial establishments suffices to increase the percentage of carbon dioxide in the air to a perceptible degree". In the past century atmospheric CO_2 rose by one third, and during this time the average land and ocean temperature increased by 1.2 °C–12.1 °C (in early 2017). Among global warming effects is the extinction of a substantial fraction of the planet's species [4], and the incidence of climate disruptions (on biodiversity, drought, major storms, etc.) is on the rise [5]. Through 2008, CO_2 was regarded as such a stable molecule that its transformation into a non-greenhouse gas posed a major challenge [6]. In 2009, we presented a solar theory termed the solar thermal electrochemical process (STEP) energy, which incorporates sub-band gap energy, unused by solar cells, to greatly improve the efficiency of CO_2 splitting [7].

In 2010 we demonstrated efficient splitting of CO_2 in a molten lithium carbonate electrolyte into both solid carbon (at 750 °C) and

* Corresponding author.
Email address: slicht@gwu.edu (S. Licht)

http://dx.doi.org/10.1016/j.mtener.2017.07.003
2468-6069/

carbon monoxide (at 950 °C) products using the STEP solar energy conversion, via an efficient (37%) concentrator photovoltaic cell that becomes even more solar efficient by directing the unused solar thermal component of sunlight to heating the molten carbonate electrolyte [8]. Subsequent to this, alternative high temperature STEP redox chemistries were developed for the generation of a number of staple products including ammonia, organics, calcium oxide, iron and methane fuel [9–16]. Such fuels from sunlight including methane, syngas, or a coal equivalent [9,10,15], are in the value range of $100 per ton product. CO_2 synthesized fuels have the disadvantage that the consumed fuel will release the captured CO_2 back into the atmosphere, and from a value perspective such fuels from sunlight provide little or no financial incentive for CO_2 mitigation. A more valuable product from than fuels or plastics is needed to provide an incentive to remove the greenhouse gas carbon dioxide.

Prior to 2015, the electrochemical synthesis of CNTs had not been widely explored. Solid carbon had been electrochemically converted to a nanostructure mix of carbon nanotubes and clustered spheroidal carbon nanoparticles in molten halide solutions via electrolytic alkali metal formation, which intercalates in and exfoliates the carbon [17]. Mixed alkali carbonate salts melt at lower temperature than the 723 °C melting point of lithium carbonate. However, a CNT electrolysis product was not observed for either a eutectic Li/K carbonate from 540 to 700 °C [18], or a eutectic Li/Na/K carbonate at 500 °C [19]. We later observed that the latter molten electrolyte does yield a small fraction of CNTs as the temperatures increases above 650 °C, but this remains a small fraction of the total electrolysis carbon product even at 750 °C [20]. Carbon electrodes in molten LiCl continued to be studied [21]. A study of 5–10% Li_2CO_3 in molten chloride concluded that "production of CNTs and nano-fibers by electrolysis in molten lithium carbonate is impossible" because "reduction and carbon deposition occurred by Li discharge and intercalation into the cathode [22]." That assessment was correct, but did not anticipate the alternative transition metal nuclei growth mechanism paths from molten Li_2CO_3 observed here (including the new multi-transition metal facilitated pathway).

In 2015, we presented the high yield, low energy electrolytic splitting of CO_2 to carbon nanofibers and nanotubes by molten lithium carbonate electrolysis [23,24], and demonstrated that the less expensive natural carbon isotope mix ($^{12}C_{0.99}{}^{13}C_{0.01}O_2$, rather than $^{13}CO_2$) produced the more expensive (carbon nanotube, rather than nanofiber) product [25], and also that CNTs are formed at high yield not only in pure Li_2CO_3, but also in mixed Li/Na, and Li/Ba and/or Ca molten carbonate electrolytes [20,26]. We have termed this high yield, molten carbonate electrolytic transformation of CO_2 to CNTs as the C2CNT process. However, the complex synthesis involved (i) a zinc coated steel cathode, (ii) a pre-CNT low current activation process to initiate the cathode nucleation, and then generated useful, but only shorter (<100 μm length) CNTs. High yield, low electrolysis voltage, and high uniformity CNTs, as produced from CO_2 dissolved in a variety of alkali and alkali-earth carbonate electrolytes, were demonstrated [20,26], and high conductivity CNTs, such as boron and other doped CNTs are readily formed by the controlled addition of impurities to the electrolyte during the electrosynthesis as exemplified (see section III in Ref. [27]). Due to the expense, energy intensity and complexity of the conventional chemical vapor deposition (CVD) synthesis and direct spin methodologies, industrial CNTs currently are valued in the $100 K ($85–$450 K) per ton range [1,28–30] and do not use CO_2 as a reactant. In C2CNT, when flue gas is provided as a reactant, a hot CO_2 source for CNTs is provided and the greenhouse gas transforms to a useful product. The electrolysis, constrained by the 4 e- reduction consumes as little as $50 of electricity per ton of CO_2 when the oxy-fuel energy improvement is taken account (the oxy-fuel improvement uses the O_2 by-product of the CNT production to improve tenergy generation efficiency) [31,32].

2. Results and discussion

Fig. 1 illustrates the new C2CNT methodology advances compared to prior C2CNT molten carbonate electrosyntheses. The first CNT wool from CO_2 by molten carbonate electrolysis is demonstrated, as seen to the right of "B" on the figure, suitable for weaving into carbon composites and textiles. 100× longer CNTs grow on Monel versus copper. Monel cathodes, electrolyte equilibration, and a mixed metal nucleation facilitate the synthesis. The previous synthetic pathway led to only short CNTs. As seen to the right of "A" on the figure, longer electrolyses had previously produced only thicker and more convoluted, but not longer, CNTs [20]. That methodology was dependent on a zinc coated steel cathode, a pure Ni anode, and a low current pre-electrolysis activation step [20,23–26]. As delineated (see section 2 in Ref. [27]), an intermediate, C2CNT electrolysis explored here, removes the requirement of a zinc coating leading to the exploration of a variety of new electrolysis bare cathode substrates, but requires the addition of Ni metal powder directly to the molten carbonate electrolyte. On the figure right side, the optimized C2CNT methodology is more straightforward and produces a high yield of macroscopic length CNT wool. Monel cathodes and Nichrome anodes are effective, and subsequent to molten electrolyte equilibration for 24 h, the C2CNT electrolysis is conducted directly without pre-electrolysis activation steps. We have previously measured that molten lithium carbonate requires several hours to achieve an equilibrium concentration of 0.29 ± 0.04 m Li_2O at 750 °C in accord with step [23,24]: $Li_2CO_3 \rightleftharpoons Li_2O + CO_2$. Sufficient electrolyte equilibration time is observed to be a significant determining factor in C2CNT growth of uniform CNT wool. Oxide/peroxide/superoxide speciation in molten carbonates is complex, time and cation dependent, and affects electrochemical charge transfer in this media. For example between 727 °C and 827 °C, the relative proportions of oxide, peroxide and superoxide in Li, Li/Na. Li/K & Li/Na/K carbonate exhibit no superoxide (<0.01%), while Na/K carbonate contains ~45% superoxide. While the oxide dominates in the pure Li electrolyte (with 99.97% oxide relative to peroxide), this proportion is 98%, 96%, 95% and only 10% respectively in Li/Na. Li/K & Li/Na/K and Na/K carbonates [33].

Fig. 2 presents the observed propagation (top) and proposed alternative growth mechanism (bottom) of the macroscopic CNT wool introduced in this study. A molten Li_2CO_3 is aged one day at 770 °C, and then a Nichrome anode and a Monel cathode immersed, and at 770 °C electrolysis is conducted at constant current (in this case 0.1 A cm^{-2}). Initially a thin carbon (as confirmed by EDS) coating forms on the Monel cathode substrate surface. The carbon coating is thin as confirmed by the relative transparency to e- beam in the SEM. We have observed that this layer is even thinner when grown on pure copper (not shown). We suggest that this opens a pathway to the ready electrochemical synthesis of graphene sheets in molten carbonates (the topic of a later study). Complete coverage of the substrate by this graphene coating under continuous applied electrolysis current is self-terminating This component of the growth is similar to the previously observed Stranski-Krastanov thin film growth, and Volmer−Weber island growth CVD growth regimes [34,35] that control the stacking order in graphene bilayers [36]. As illustrated in the bottom Fig. 2, and consistent with the observed SEM CNTs grow outward from the layered graphene peeled (from the monel) morphology in the upper portion of that figure at transition metal catalyst

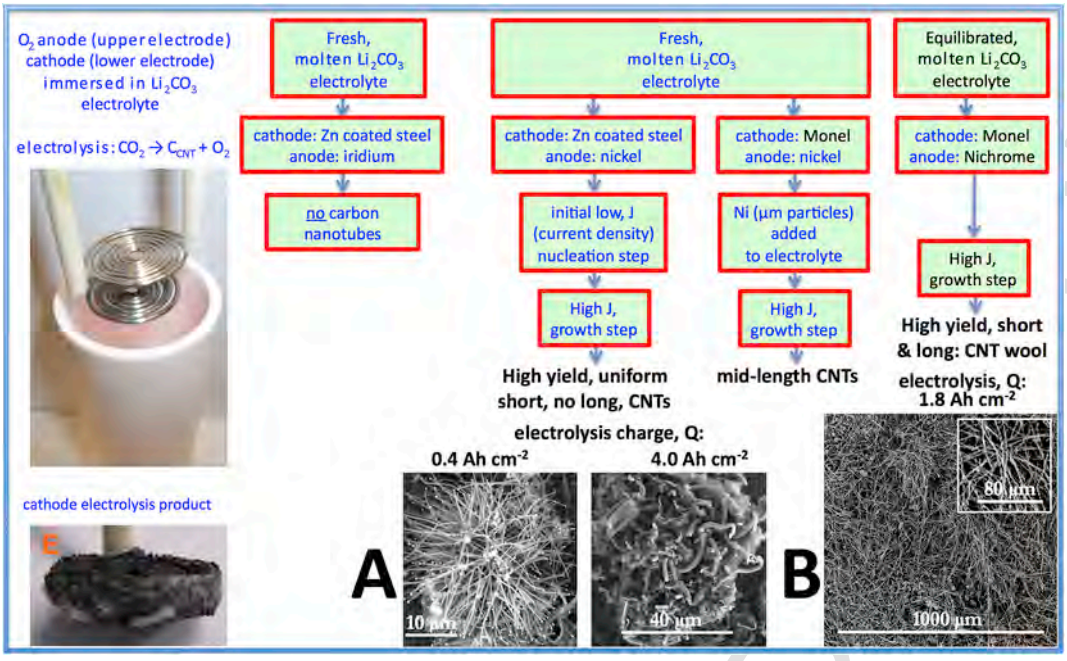

Fig. 1. Schematic representation of new synergistic pathways to form a high yield of macroscopic length CNT "wool" by electrolysis in molten carbonate. Middle: Prior C2CNT syntheses were dependent on a zinc coated steel cathode, a pure Ni anode, and a low current pre-electrolysis activation step. An intermediate, new C2CNT electrolysis removes the requirement of a zinc coating leading to the exploration of a variety of new cathode substrates. Right side: The optimized C2CNT pathway utilizes Monel cathodes and Nichrome anodes, molten electrolyte equilibration for 24 h, and the electrolysis is conducted directly without pre-electrolysis activation steps. This pathway produces a high yield of macroscopic length CNT wool. Left side: experimental cell configuration used in these C2CNT experiments.Larger cells are shown in sect. IV of Ref. [27].

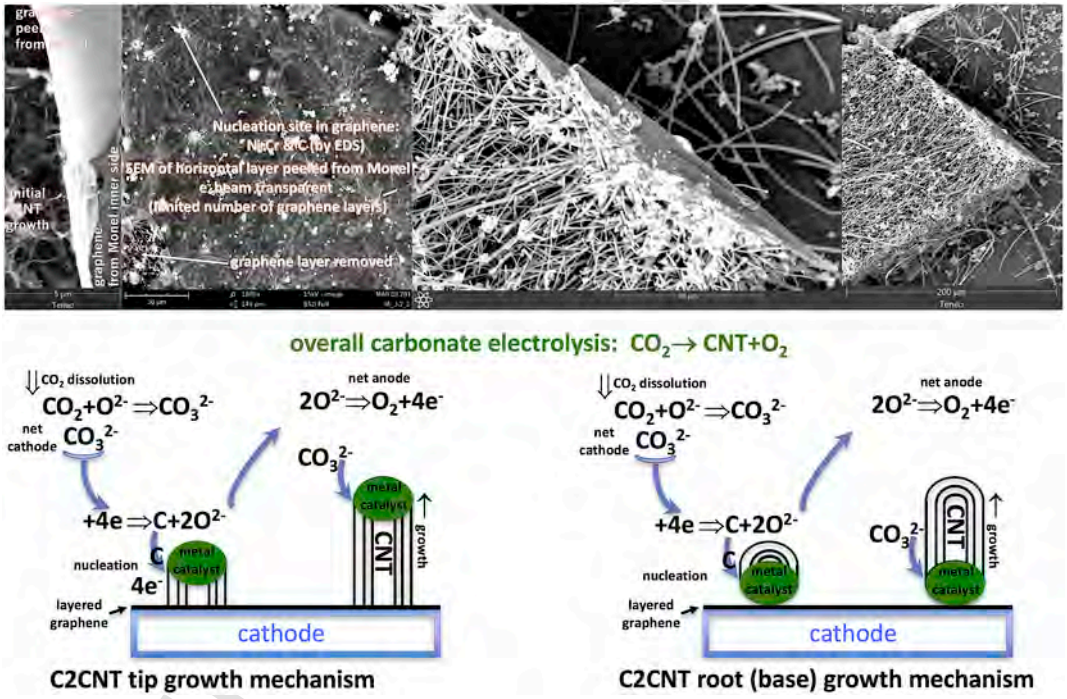

Fig. 2. Top: SEM of product formed in the initial electrolysis stages at the Monel cathode/equilibrated electrolyte interface. Bottom: Carbonate electrolytic growth model of carbon nanotubes from CO_2. The mechanism of electrolytic synthesis of CNTs had not been previously elucidated and here is based on the layered graphene observation observed in the top of the figure, and our previous SEM, EDX, TEM, chemical balance (the oxide buildup when CO_2 is excluded), DFT calculations, and isotopic evidence. This proposed tip (left) or base (right) mechanism occurs at the solid/liquid (molten carbonate) interface, and transforms CO_2 into CNTs. The mechanisms are analogous to the CVD growth mechanism, which instead occurs at the solid/gas, interface, and transforms organics, rather than CO_2, into CNTs.

sites. As delineated (see section I in Ref. [27]) (i) certain combinations of transition metals catalysts lead to CNT growth and repair that are 10–100 fold better than single metals alone, (ii) copper containing cathodes can improve the uniformity of the base graphene layer to initiate CNT growth, and (iii) the CNT growth may be dominated by growth from a catalyst tip (Fig. 2 bottom left) that maximizes exposure to the bulk electrolyte and will minimize bulk carbon(IV) diffusion constraints, rather than the catalyst root/base (Fig. 2 bottom right) growth mechanism. The morphology of carbon nano-particle growth is highly dependent on the initial metal substrate and the transition metals available to act as nucleation growth points. It is observed (by EDS analysis of the elemental composition at localized points on the graphene coating) that transition metals form nucleation points, which initiate growth of the observed grown CNTs. Here, the source of the transition metals is the low-level oxidative release from the anode. For example, nickel, Ni^{2+} is soluble, but only at ppm concentrations in these molten carbonate electrolytes [37], and the anodic release of Ni^{2+} slows as a stabilized nickel oxide layers forms on the anode surface [38]. Both nickel, chromium and iron are available when NiChrome, rather than pure nickel (Ni 200) is used as the anode. This availability as co-nucleation metals results in the most uniform, consistent and longest CNTs we have electrosythesized to date.

Fig. 3 presents the high quality CNT wool product consistently obtained in replicate syntheses subsequent to cathode extraction and washing after an 18-h electrolysis at 0.1 A cm^{-2} under these electrolysis conditions (Monel cathode, Nichrome anode, 24 h equilibrated 770 °C Li_2CO_3). The carbon product is immediately observed to be different than that from our prior molten carbonate electrosyntheses. This product is wool-like and fluffy, rather than the powdery or sandy. In the figure, this difference is evidenced by the macroscopic length (100 fold longer) than the prior 5–50 μm length of previous syntheses. As with previous, optimized C2CNT electrosyntheses, the typical C2CNT coulombic yield (in which 100% is equivalent to a 4 e- conversion of all applied charge reducing the tetravalent carbon) is >90% (and higher with careful product recovery). Additionally, in the case of the new, synthesis the carbon product consists of ~95% macroscopic CNTs. As seen in figure, the CNT product ranges 0.4–1.2 mm long. Optical (not shown) microscopy, rather than SEM, of the same product shows several outlier CNTs that are over 2 mm long. As seen in the lower portion of Fig. 4, the inter-graphene sepa-

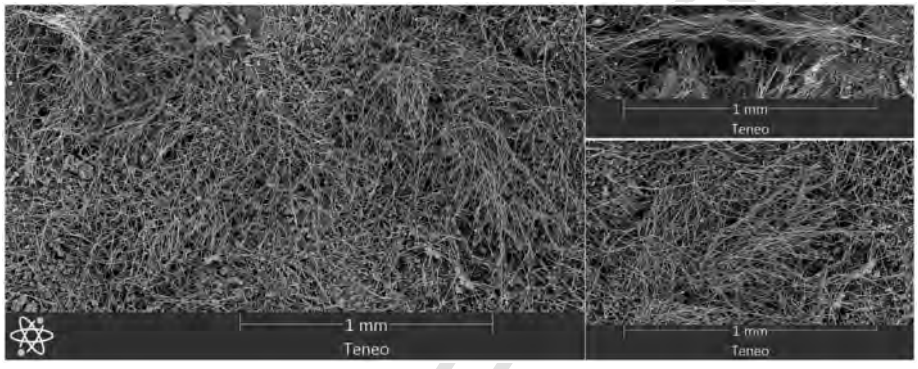

Fig. 3. SEM of the CNT wool product produced at the cathode from CO_2 during replicate syntheses of 770 °C Li_2CO_3 electrolysis. Electrolysis is for 18 h at 0.1 A cm^{-2} (1.8 Ah cm^{-2}) between a NiChrome anode and a Monel cathode.

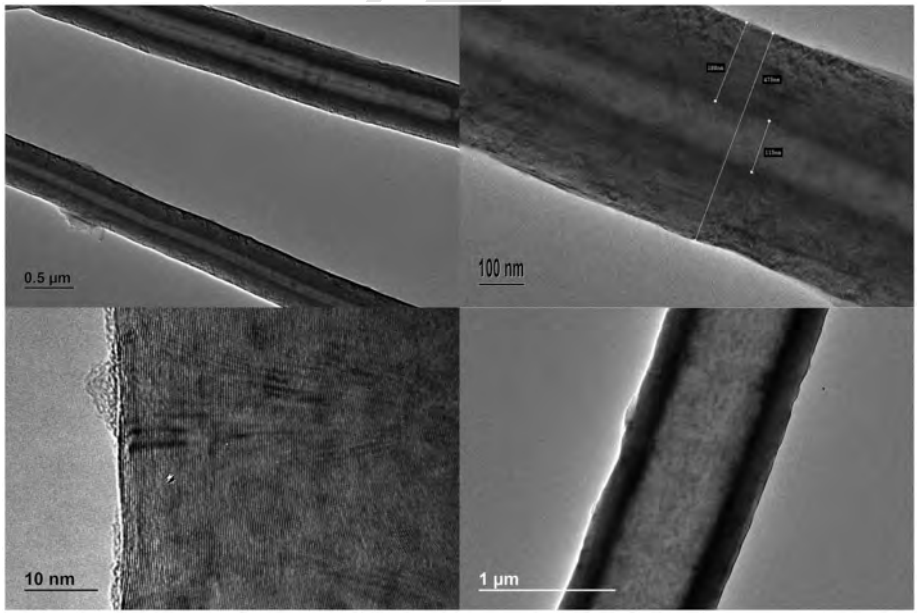

Fig. 4. TEM presenting the range of these C2CNT generated CNT diameters. The lower left 10 nm scale TEM presenting the inter-graphene wall spacing is from our reference [25].

ration of the CNTs' walls by TEM exhibits the typical 0.342 nm variation [25], and the CNTs' diameters ranges from 0.5 to 1.5 μm. The inner diameter of the tubes varies by as much as a factor of three. As we have recently demonstrated, we will be able to refine and further minimize the range of these parameters by careful control of the electrolyte composition, temperature and current density [26].

3. Discussion

A synthesis is introduced that forms the first electrolytic CNT wool and consists of a hundred-fold increase in the length of molten carbonate electrolyte CNTs. 100x-longer CNTs grow on Monel versus steel. Monel, electrolyte equilibration, and a mixed metal nucleation facilitate the synthesis. CO_2, the sole reactant in this transformation, is directly extractable from dilute (atmospheric) or concentrated sources, and as delineated by the analyzed C2CNT production cost of $660 per ton CNT (see section IV in Ref. [27]), this CNT is cost constrained only by the (low) cost of electricity. Our experiments here on the widely varying carbon morphologies produced at different cathode substrates during molten carbonate electrolysis is delineated (see sections I-III in Ref. [27]), the ready addition of heteroatoms during the electrolysis, to achieve CNTs with difference properties, intermediate stages of the C2CNT synthesis methodology advance and the scalability of the C2CNT process. The low electrical cost, ease of synthesis and wide range of uniform CNTs accessible by C2CNT provide an economic incentive to treat CO_2 as a resource, rather than a pollutant, to encourage removal of this greenhouse gas to mitigate climate change.

Efficacious climate mitigation by CO_2 transformation requires a massive market, and product stability and compactness. The most compact form of captured carbon is through its transformation to solid carbon. CNTs are among the highest strength and most stable materials. CNT cost reduction by C2CNT, provides a preferred (lower mass per unit strength) to the mass metal market, and the CNT wool introduced here accelerates CNT demand as a building industry and textile material. Together these principal societal staples, when produced from CO_2, comprise an ample demand to markedly decrease atmospheric carbon. Scalability of the C2CNT process is delineated (see section IV in Ref. [27]). Initial scaling is efficiently applied to available concentrated, hot sources of CO_2, such as eliminating the CO_2 emission from industrial smoke stacks and simultaneously forming valuable CNT wool. Larger scale C2CNT can be achieved through direct elimination of atmospheric CO_2 using solar heat and solar to electric PVs. We have calculated that a surface area equivalent to less than 10% of the Sahara Desert is sufficient to remove all excess anthropogenic CO_2 by carbonate electrolysis in ten years, but open ocean areas may provide a more available surface. Heat exchange, between pretreated and CO_2 extracted air will be formidable; this may be facilitated with saltwater separation of salts and fresh water, as schematically represented in Fig. 5.

4. Experimental procedures

Electrolyses are driven galvanostatically in 50 g of 770 °C molten lithium carbonate (99% Alfa Aesar). The electrolysis is contained in a pure alumina crucible (AdValue 99.6%). A variety of metals are explored as alternative cathodes and coiled as spiraled wires to form a horizontal flat disc of area 5 cm^2. Above this is a comparable, parallel anode as 5 cm^2 coiled wire of either pure nickel (Ni 200) or NiChrome wire. CO_2 pre-concentration is not required. During electrolysis, a carbon product accumulates at the cathode and oxygen evolves at the anode in accord with a CO_2 splitting reaction. We have previously utilized ^{13}C isotope CO_2 to track and demonstrate that CO_2 originating from the gas phase serves as the renewable carbon building blocks in the observed CNT product [25] and the net reaction is in accord with:

$$\text{Dissolution: } CO_2(\text{gas}) + Li_2O(\text{soluble}) \rightarrow Li_2CO_3(\text{molten}) \quad (1)$$

$$\text{Electrolysis: } Li_2CO_3(\text{molten}) \rightarrow C(\text{CNT}) + Li_2O(\text{soluble}) + O_2(\text{gas}) \quad (2)$$

$$\text{Net: } CO_2(\text{gas}) \rightarrow C(\text{CNT}) + O_2(\text{gas}) \quad (3)$$

Subsequent to electrolysis the product remains on the C2CNT cathode, but falls off with congealed electrolyte when a coiled wire

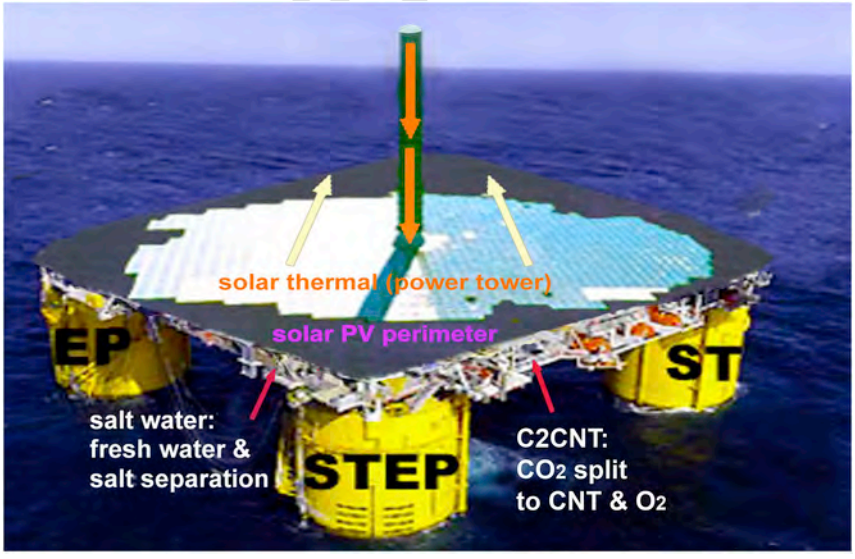

Fig. 5. Schematic representation of a solar thermal and photovoltaic field to drive both water purification and C2CNT splitting of CO_2 to useful products.

cathode is extracted, cooled, and uncoiled, or simply pealed off from a planar Monel cathode. Processes that help avoid electrolyte congealing on the product and tend to exclude molten electrolyte while extracting the product hot include (i) bubbling gas through the cathode. One means by which this is accomplished is by increasing the temperature while continuing the end of the electrolysis. There is a smooth transition from the solid carbon cathode reduction product in the 700 °C range to gaseous carbon monoxide in the 900 °C range, and intermediate temperature allows their co-formation, At 850 °C and 900 °C the solid carbon to the CO product ratios were observed to be 2:1 and 0.5 to 1, respectively and at 950 °C CO is the sole product [8]. Alternatively, at, and near, the electrolysis temperature, the viscous carbon/electrolyte mix on the cathode readily scrapes off the cathode, and a second method is (ii) the filtration of the hot molten electrolyte/carbon product mix through a high mesh size, small pore filter (such as nickel, nickel alloy, steel or ceramic) which we observe separates carbon clusters from molten electrolyte; in this regards, a hot solid state molten electrolyte absorbent in contact under the filter is particularly effective at drawing out the molten electrolyte (we utilize BNZ 2300 firebricks which are temperature resistant and porous). Reversing polarity of the electrodes can generate O_2 to drive out electrolyte, although this competes with oxidation of the carbon product. Several aqueous washing routes are equally viable to separate any congealed (water soluble) electrolyte from the insoluble CNTs and are summarized here. Whereas the product of lithium carbonate and either formic acid or HCl acid, lithium formate or lithium chloride, have a high aqueous solubility at 20 °C, the solubility of lithium carbonate is relatively low in pure water, (respectively $LiHCO_2$, LiCl and Li_2CO_3 dissolve to 39.3 g, 83.5 g and 1.3 g per 100 g H_2O). Interesting, the solubility of lithium carbonate increases in cold water to 1.5 g at 0 °C and decreases to 0.8 g at 85 °C, but that of lithium formate and lithium chloride increase with temperature (to 138 and 128 g per 100 g H_2O respectively at 100 °C), and this higher washing temperature does not affect the stable CNT product. Hence, the product is washed with cold deionized water, or more quickly washed with small amounts of hot HCl (forming lithium chloride) or hot formic acid (forming lithium formate) to dissolve electrolyte that had congealed with the product, and the product is dried. Alternatively, we measure that the product is cleaned via lithium carbonate's higher than pure water solubility in aqueous ammonium sulfate; dissolving in 4.46 molal (moles $(NH_4)_2SO_4$ per kg H_2O) at 6.7, 6.8, 7.1 and 7.9 g Li_2CO_3/100 g H_2O at 25, 50, 75 and 100 °C. Ammonium sulfate solubility increases with temperature, to 6.45 m at 100 °C and 6.64 m at 108.5 °C, and also dissolves more lithium carbonate, respectively 11.4 and 11.6 g Li_2CO_3/100 g H_2O at 100 and 108.5 °C. As a final aqueous alternative, the lithium carbonate electrolyte is removed as lithium bicarbonate ($LiHCO_3$, formed as aqueous Li_2CO_3 under higher CO_2 partial pressure than in air, for example Li_2CO_3 under 1 bar of CO_2 has a 20 °C solubility of 4.6 g per 100 g H_2O). In this latter case, the CNT product is washed at higher pressure which dissolves out the Li_2CO_3 as the bicarbonate. The washing solution is then removed to lower pressure, which then separates, by precipitation, Li_2CO_3. This high/low pressure sequence cycle is repeated as necessary.

The washed carbon product is analyzed by PHENOM Pro-X Energy Dispersive Spectroscopy (EDS) on the PHENOM Pro-X SEM or FEI Teneo LV SEM and by TEM with a JEM 2100 LaB6 TEM. Raman spectroscopy was measured with a LabRAM HR800 Raman microscope (HORIBA) using 532.14 nm wavelength incident laser light with a high resolution of 0.6 cm^{-1}. The synthesis yield, $100\% \times C_{experimental}/C_{theoretical}$, is determined by the measured mass of washed carbon product removed from the cathode, $C_{experimental}$, and the theoretical mass, $C_{theoretical} = (Q/nF) \times (12.01\ g\ C\ mol^{-1})$ which is determined from Q, the time integrated charged passed during the electrolysis, F, the Faraday (96485 As mol^{-1} e^-), and the n = 4 e-mol^{-1} reduction of tetravalent carbon. Further details are presented (see sections Iand II in Ref. [27]).

Author contribution

Conceptualization: S.L.; Methodology: All authors; Investigation: All authors.

Writing: S.L.; Supervision: S.L.

Acknowledgments

We are grateful to the United States National Science Foundation grant 1505830 for partial support of this study.

References

[1] Cheaptubes.com, Cheaptubes: Industrial Grade Carbon Nanotubes, 2017, Available from: https://www.cheaptubes.com/product-category/industrial-carbon-nanotubes-products/.

[2] CO2-earth, Daily CO2 Values, 2017, May 2017 CO2 levels from: https://www.co2.earth/daily-co2.

[3] NASA: Global Climate Change, Global Climate Change: the Relentless Rise of Carbon Dioxide. NASA: Global Climate Change, 2017, Available from: https://climate.nasa.gov/climate_resources/24/.

[4] M.C. Urban, Accelerating extinction risk from climate change, Science 348 (2015) 571–573.

[5] S.L. Pimm, Climate disruption and biodiversity, Curr. Biol. 19 (2009) R595–R601.

[6] G.K. Prakash, G.A. Olah, S. Licht, N.B. Jackson, Reversing Global Warming: Chemical Recycling and Utilization of CO_2, 2008, Report of 2008 NSF Workshop. Available from: http://loker.usc.edu/ReversingGlobalWarming.pdf.

[7] S. Licht, STEP (solar thermal electrochemical photo) generation of energetic molecules: a solar chemical process to end anthropogenic global warming, J. Phys. Chem. C 113 (2009) 16283–16292.

[8] S. Licht, B. Wang, S. Ghosh, H. Ayub, D. Jiang, T. Ganley, A new solar carbon capture process: STEP carbon capture, J. Phys. Chem. Lett. 1 (2010) 2363–2368.

[9] F. Li, J. Lau, S. Licht, Sungas instead of syngas: efficient co-production of CO and H_2 from a single beam of sunlight, Adv. Sci. 2 (2011) 1500260.

[10] F. Li, S. Liu, B. Cui, J. Lau, J. Stuart, S. Licht, A one-pot synthesis of hydrogen and carbon fuels from water and carbon dioxide, Adv. Energy Mater 7 (2015) 1401791-1–1401791-7.

[11] F. Li, B. Wang, S. Licht, Sustainable Electrochemical Synthesis of large grain or catalyst sized iron, J. Sustain. Metall. 2 (2016) 405–416.

[12] S. Licht, Efficient solar-driven synthesis, carbon capture, and desalinization, STEP: solar thermal electrochemical production of fuels, Met. Bleach. Adv. Mater. 23 (2011) 5592–5612.

[13] S. Licht, B. Cui, B. Wang, F. Li, J. Lau, S. Liu, Ammonia synthesis by N_2 and steam electrolysis in molten hydroxide suspensions of nanoscale Fe_2O_3, Science 345 (2014) 637–640.

[14] S. Licht, H. Wu, C. Hettige, B. Wang, J. Asercion, J. Lu, J. Stuart, STEP cement: solar thermal electrochemical production of CaO without CO_2 emission, Chem. Commun. 48 (2012) 6018–6922.

[15] H. Wu, D. Ji, L. Li, D. Yuan, Y. Zhu, B. Wang, Z. Zhang, S. Licht, A new technology for efficient, high yield carbon dioxide and water transformation to methane by electrolysis in molten salts, Adv. Mat. Tech. 1 (2016a) 160092.

[16] Y. Zhu, H. Wang, B. Wang, X. Liu, H. Wu, S. Licht, Solar thermoelectric field photocatalysis for efficient organic synthesis exemplified by toluene to benzoic acid, Appl. Catal. B 193 (2016) 151–159.

[17] W.K. Hsu, J.P. Hare, H.W. Terrones, Kroto, D.R.M. Walton, Condensed-phase nanotubes, Nature 377 (1995) 687.

[18] H. Ijije, C. Sun, G.Z. Chen, Indirect electrochemical reduction of carbon dioxide to carbon nanopowders in molten alkali carbonates: process variables and product properties, Carbon 73 (2014) 163–174.

[19] H. Yin, X. Mao, D. Tang, W. Xiao, L. Xing, H. Zhu, D. Wang, D.R. Sadoway, Capture and electrochemical conversion of CO2 to value-added carbon and oxygen by molten salt electrolysis, Energy Environ. Sci. 6 (2013) 1538–1545.

[20]

[21] A. Dimitrov, A. Tomova, A. Grodzdanov, O. Popovski, P. Paunović, Electrochemical production, characterization, and application of MWCNTs, J. Solid State Electrochem. 17 (2013) 399–407.

[22] A.T. Dimitrov, Study of molten Li_2CO_3 electrolysis as a method for production of carbon nanotubes, Maced. J. Chem. Chem. Eng. 28 (2009) 111–118.

[23] J. Ren, F. Li, J. Lau, L. Gonzalez-Urbina, S. Licht, One-pot synthesis of carbon nanofibers from CO_2, Nano Lett. 15 (2015a) 6142–6148.

[24] J. Ren, J. Lau, M. Lefler, S. Licht, The minimum electrolytic energy needed to convert carbon dioxide to carbon by electrolysis in carbonate melts, J. Phys. Chem. C 119 (2015b) 23342–23349.

[25] J. Ren, S. Licht, Tracking airborne CO_2 mitigation and low cost transformation into valuable carbon nanotubes, Sci. Rep. 6 (2016), 27760–27761-11.

[26] J. Ren, M. Johnson, R. Singhal, S. Licht, Transformation of the greenhouse gas CO_2 by molten electrolysis into a wide controlled selection of carbon nanotubes, J. CO2 Util. 18 (2017) 335–344.

[27] M. Johnson, J. Ren, Lefler, G. Licht, J. Vicini, S. Licht, Synthesis, Cost and Scale-ability of Doped, and Wool Carbon Nanotubes Made Directly from CO_2 by Molten Electrolysis: Value Driven Pathways to Greenhouse Gas Mitigation, 2017, Data in Brief, submitted.

[28] D. Janas, K.K. Koziol, Carbon nanotube fibers and films: synthesis, applications and perspectives of the direct-spinning method, Nanoscale 8 (2016) 19475.

[29] X.L. Jia, F. Wei, Advances in production and application of carbon nanotubes, Top. Curr. Chem. 375 (2017) http://dx.doi.org/10.1007/s41061-017-0102-2.

[30] A. Magrez, S. Arnaud, J. Won, R. Smajda, et al., Catalytic CVD synthesis of carbon nanotubes: towards high yield and low temperature growth, Materials 2 (2010) 487–4890.

[31] J. Lau, G. Dey, S. Licht, Thermodynamic assessment of CO_2 to carbon nanofiber transformation for carbon sequestration in a combined cycle gas or a coal power plant, Energy Conserv. Manag. 122 (2016) 400–410.

[32] S. Licht, Co-production of cement and carbon nanotubes with a carbon negative footprint, J. CO2 Util. 18 (2017) 378–389.

[33] M. Cassir, G. Moutiers, J. Devynck, Stability and characterization of oxygen species in alkali molten carbonate: a thermodynamic and electrochemical approach, J. Electrochem. Soc. 140 (1993) 3114–3123.

[34] D.J. Eadlesham, M. Cerullo, Dislocation-free Stranski-Krastow growth of Ge on Si(100), Phys. Rev. Lett. 64 (1990) 1943–1946.

[35] M. Yan, H.T. Zhang, E.J. Widjaja, R.P.H. Chang, Self-assembly of well-aligned gallium-doped zinc oxide nanorods, J. Appl. Phys. 94 (2003) 5240–5246.

[36] H.Q. Ta, D.J. Perello, D.L. Duong, G.H. Han, S. Gorantla, V.L. Nguyen, A. Bachmatiuk, S.V. Rotkin, Y.H. Lee, Ru¨mmeli M.H. Stranski-Krastanov, Volmer-Weber, CVD growth regimes to control the stacking order in bilayer graphene, Nano Lett. 16 (2016) 6403–6410.

[37] D.-G. Lee, K. Yamada, T. Nishina, I. Uchida, In situ NiO dissolution behavior in $(Li+Na)CO_3$ melts under pressurized oxidant gas atmospheres, J. Power Sources 62 (1996) 145–147.

[38] S. Licht, H. Wu, STEP iron, a chemistry of iron formation without CO_2 emission: molten carbonate solubility and electrochemistry of iron ore impurities, J. Phys. Chem. C 115 (2011) 25138–25147.

Data article

Synthesis, Cost and Scale-ability of Doped, and Wool Carbon Nanotubes Made Directly from CO_2 by Molten Electrolysis: Value Driven Pathways to Greenhouse Gas Mitigation

M. Johnson[1], J. Ren[1], M. Lefler[1], G. Licht[1], J. Vicini[1], S. Licht[1,*]

[1]Dept. of Chemistry, George Washington University, Washington DC 20052.

Contact email: slicht@gwu.edu

Abstract

This data provides a benchmark for carbon nanotubes synthesized via molten electrolyte via the carbon dioxide to carbon nanotube (C2CNT) process useful for comparison to other data on longer length C2CNT wools; specifically: (I) C2CNT electrosynthesis with bare (uncoated) cathodes and without pre-electrolysis low current activation. (II) C2CNT Intermediate length CNTs with intermediate integrated electrolysis charge transfer. (III) C2CNT Admixing of sulfur, nitrogen and phosphorous (in addition to boron) to carbon nanotubes, and (IV) Scalability of the C2CNT process.

Specifications Table

Subject area	*Chemistry*
More specific subject area	*Carbon Nanotubes and Climate Change Mitigation*
Type of data	*SEM, TEM, Raman Spectra, Conductivity, Schematics, Cost Analysis*
How data was acquired	*PHENOM Pro-X SEM with EDS or FEI Teneo LV SEM, JEM 2100 LaB6 TEM, LabRAM HR800 HORIBA Raman Spectrometer*
Data format	*Raw and analyzed data is presented*
Experimental factors	*Analyzed cathode product is washed to remove congealed electrolyte*
Experimental features	*CO_2 is electrolyzed in molten carbonate forming carbon nanotubes*
Data source location	*Washington, DC, USA*
Data accessibility	*Data is accessible in this article format*

Value of the data

This data provides a benchmark for carbon nanotubes synthesized via molten electrolyte via the carbon dioxide to carbon nanotube (C2CNT) process useful for comparison to other data on longer length C2CNT wools; specifically:

- C2CNT electrosynthesis with bare (uncoated) cathodes and without pre-electrolysis low current activation.
- C2CNT intermediate length CNTs with intermediate integrated electrolysis charge transfer.
- C2CNT admixing of sulfur, nitrogen and phosphorous (in addition to boron) to carbon nanotubes.
- Scalability of the C2CNT process.

Data

This data associated with a research study (Johnson, in press) provides a benchmark for carbon nanotubes synthesized using a molten carbonate electrolyte from carbon dioxide using the C2CNT (CO_2 to carbon nanotube) process useful for comparison to other data on longer length C2CNT wools.

Experimental Design, Materials and Methods

I. C2CNT electrosynthesis with bare (uncoated) cathodes and without pre-electrolysis low current activation:

In the initial electrosynthetic methodology (Ren, Li 2015; Ren, 2017 and references therein), the cathode consists of a galvanized (zinc coated) steel electrode, and an initial low current (0.05 A (amps) for 10 minutes, 0.1 A for 10 minutes, 0.2 A for 5 minutes, and 0.4 A for 5 minutes) series of steps is applied to grow Ni nucleation sites on the cathode, followed by a longer, constant current (controlled at 0.1 to 0.2 A cm^{-2}). As one example of the initial methodology the electrolysis is conducted with a lithium metaborate additive to the electrolyte, that is to the 50 g of Li_2CO_3, either 1.5 g, 3 g, 5 g, 8 g, or 10 g of $LiBO_2$ is added to the electrolyte. The SEM observed morphology of the products remains unchanged with these various levels of $LiBO_2$ addition, and consists of 5 to 50 µm long carbon nanotubes (CNTs) as exemplified on the left of Figure 1. The boron addition to the electrolyte boron-dopes the CNTs (as determined by a Raman peak shift in the G band (Ren, 2011) seen in the top right of Figure 1) and increases their electrical conductivity by a factor of ten as summarized in the bottom right of Figure 1.

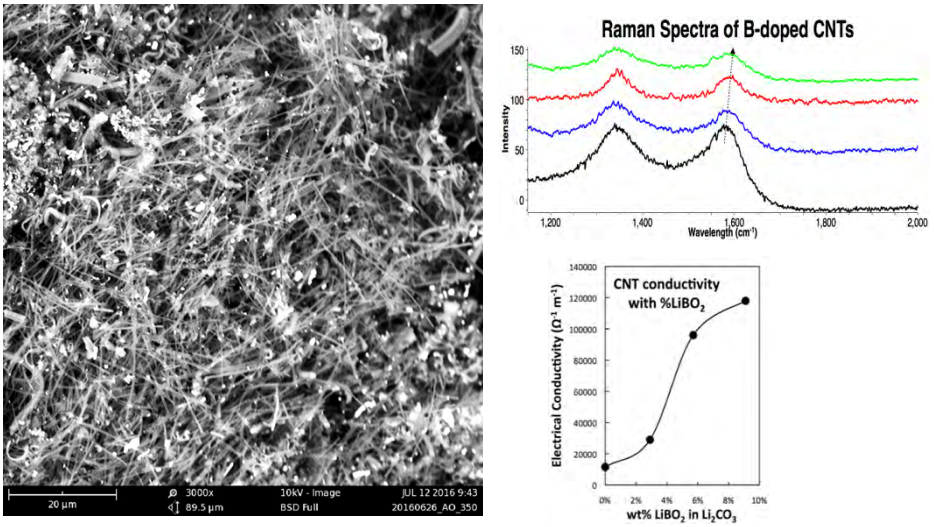

Figure 1. Properties of boron doped CNTs formed by electrosynthesis in molten carbonate. SEM (top) and Raman spectra (left) of B-doped CNTs formed by 1 Ah electrolysis at a 5 cm^2 cathode in 5 g $LiBO_2$ and 50 g Li_2CO_3 at 770°C. Right: the electrical conductivity of CNTs grown with an increasing concentration of $LiBO_2$ dissolved in the Li_2CO_3 electrolyte. Note that we had previously reported the anode and cathode surface area each as 10 cm^2. More specifically this was the total (two sided) exposed surface area, whereas the surface area facing each electrode is 5 cm^2.

Several combined carbon dioxide to carbon nanotube (C2CNT) effects (elimination of the

cathode zinc coating and pre-electrolysis activation steps, cathode substrate composition, electrolyte aging, and choice of anode substrage composition) lead to the first production of CNT wool. In this data, the first several of these effects effects (removal of the cathode zinc coating effect, elimination of the pre-electrolysis low-current activation steps and cathode substrate composition choice) are shown. As a first step towards the new synthesis electrolyses are conducted without zinc coated cathodes, which had been considered as a necessary component to the synthesis (Dey, et al., 2016; Ren, et al., 2015; Ren, et al., 2017; Ren and Licht, 2016; Wu, 2016, Licht, et al., 2016), but instead with fine (3-5 μm) Ni metal powder added directly as additional transition metal to the electrolyte to compensate for the lack of the zinc activating agent. Less than 1% by mass added Ni was sufficient (0.1 to 10% Ni addition was explored, and larger than 5 μm added Ni powder was less effective than the 2-5 μm powder) to promote CNT growth. Removal of the zinc coating constraint opens the pathway to explore other (than steel) metals as cathode substrates and in particular certain metal substrates promoted a longer CNT product. The previous galvanized steel cathode had a zinc coating and as zinc has a 420°C melting point which is less than the temperature of the molten electrolyte ($\geq$ 750°C) in which the cathode is immersed, liquid zinc could form. In that case the liquid zinc could leave the electrode and helps initiate the dissolution of nickel from the anode or formation of carbon (Ren, et al., 2015; Ren, et al., 2017; Ren and Licht, 2016; Wu, 2016). In lieu of the zinc, the direct, addition of Ni powder to the electrolyte provides sharper control of the initiation of CNT growth than the previous methodology which utilized the release of Ni during the initial gradual formation of a stable Ni oxide layer at the anode which had been observed to require a gradual increase of electrolysis current to yield a high formation of the CNT product at the cathode. Here the higher steady-state electrolysis current can be initially and continuously applied without the need for that lower current density activation of CNT growth.

As seen in Figure 2 by SEM of the cathode product, even a low level (0.1 wt%) of the Ni powder added to the Li_2CO_3 electrolyte promotes CNT growth. To ensure that no Ni is in the system other than that added as Ni powder, an iridium anode, rather than Ni or Ni alloy anode, was used in this electrosynthesis, and we've previously noted that Ir is also an effective (albeit expensive) oxygen electrode for the carbonate system. As seen in the top panel of the figure, without the Ni powder (and without the zinc cathode coating) no CNT product is observed. However, with the added Ni powder (and still without the zinc cathode coating), in the middle amd lower panels, it seen these product CNTs are highly uniform and of high purity CNTs.

Each of the subsequent experiments in this data are conducted on various cathodes, each by electrolysis with 0.4 wt% of 3-5 μm Ni powder utilized in the 770°C molten lithium carbonate and in each case the electrolyses were conducted at constant current (without an initiating series of activation increasing constant current steps). As seen in Figure 3, while Monel and copper both produce a high yield of CNTs, the CNT morphology is entirely different after 1.5 hours of electrolysis time (at 1-amp constant current between the 5 cm^2 electrodes). The copper cathode forms thin, tangled CNTs, while the Monel cathode forms uniform, thicker and straight CNTs. A pure Ni cathode (not shown) produces a CNT similar to that of copper although the CNT yield (80 to 85%) is less than that of the $\geq$ 85% yield of the copper cathode. As shown on the left side of Figure 4, a Nichrome cathode provides straighter CNTs than a pure nickel cathode. The nickel chromium cathode continues to produce straight CNTs during intermediate duration electrolyses, but unlike the Monel cathode CNTs from a nickel chromium substrate cathode did not continue to grow during extended electrolytes. Iron oxide (unlike nickel oxide)

is highly soluble in molten carbonate and we have previously shown that its addition to the electrolyte generates an uncontrolled growth of a profusion of nanostructures (Ren, et al., 2015; Ren, et al., 2017; Ren and Licht, 2016; Wu, 2016). A pure iron cathode substrate generates a similar heterogeneous product as seen in the right side of Figure 4. Figure 5 presents the product generated at several different cathodes subsequent to extended (12 Ah) electrolyses. As seen a titanium cathode yielded shorter and only moderate quality CNTs, while a graphite foil cathode yielded high quality, but shorter (than a Monel Cathode) CNTs subsequent to these extended electrolysis.

Of the eight cathodes examined (Monel, steel, iron, nickel, nickel chromium, copper, titanium, and graphite) only Monel exhibited a CNT product whose length increases (and was approximately linear) with the increase in integrated electrolysis charge density. Another eight other similar alloys from Online Metals (online metals.com) were acquired for further data comparison consisting of:

(i) Nickel silver (55% Cu, 27% Zn, 18% Ni) from Online Metals (online metals.com)
(ii) Brass 260 (70% Cu, 30% Zn) Online Metals
(iii) Naval Brass 464 (61% Cu, 39.25% Zn, 0.75% Sn) Online Metals
(iv) Ni K500 (>63% Ni, 27-33% Cu, 2.3-3.15% Al, max 2.0% Fe, 1.5% Mn, 0.5% Si) Online Metals
(v) Cu 182 (99.1% Cu, 0.9% Cr) Online Metals
(vi) Munz metal (brass) (61% Cu, 40% Zn, trace iron) Online Metals
(vii) Cu 715 (30% Ni, 70% Cu) MARMETAL
(viii) Cu 706 (10% Ni, 90% Cu) MARMETAL

Subsequent to 770°C molten lithium carbonate electrolysis the Munz brass produces CNTs of macroscopic dimensions approaching, but not as large as, the Monel cathode, as another example the 30% Ni, 70% Cu alloy produces a single product CNTs containing both short and macroscopic reminiscent of both pure Cu and Monel.

Subsequent to the initial screening of the electrolysis cathode substrate, two further significant advances to the C2CNT process were found. 1) Uncoated (bare, without zinc) substrate cathodes can generate a CNT product without any Ni powder added to the electrolyte, when the molten electrolyte is "aged" (left molten prior to electrolysis) for 24 hours prior to electrolysis (longer periods did not further improve CNT quality). The low level of nickel dissolving from the anode is sufficient to migrate and act as nucleation at the cathode, and this originates while the anodic nickel oxide layer is established at the start of the electrolysis. 2) The quality (length and quantity of CNT) improves when the anode consists of Nichrome (Nichrome 60, also referred to as Chromel C (60% Ni, 16% Cr, 24% Fe)), rather than a pure nickel anode, and both Ni and Cr are then observed by EDS at the cathode CNT nucleation sites.

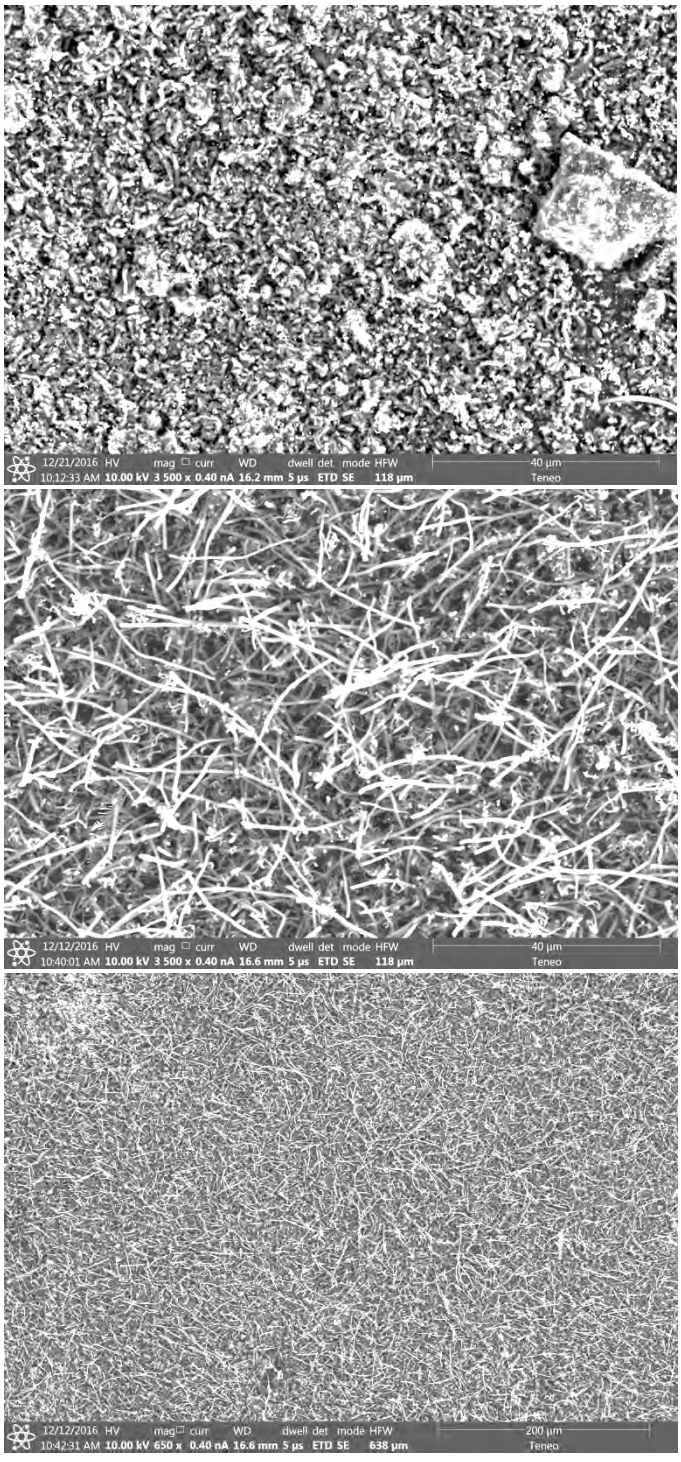

Figure 2. Top: In the absence of added Ni powder, a bare (zinc free) cathode does not form an observable CNT electrolysis product from a fresh molten Li_2CO_3 electrolyte, but with appropriate choice of substrate can form a highly uniform CNT product (middle and lower panel) with the addition of a low level (0.1 wt%) 3-5 µm Ni powder to the electrolyte. 1.2 Ah cm^{-2} electrolyses are conducted using an Ir anode (rather than Ni anode, to ensure the anode does not introduce nickel to the electrolyte) and a Monel cathode in 770°C Li_2CO_3.

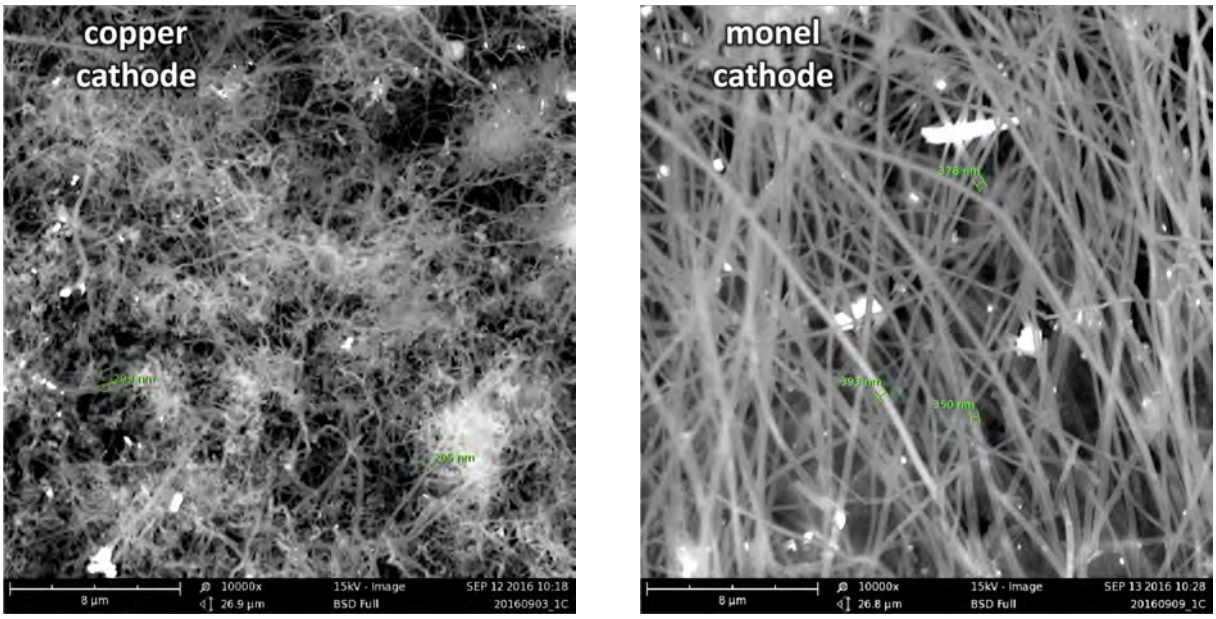

Figure 3. Comparison of the CNT product formed respectively at a copper (left side) and Monel (right side) cathode during short duration 0.3 Ah cm^{-2} electrolysis in 770°C Li_2CO_3.

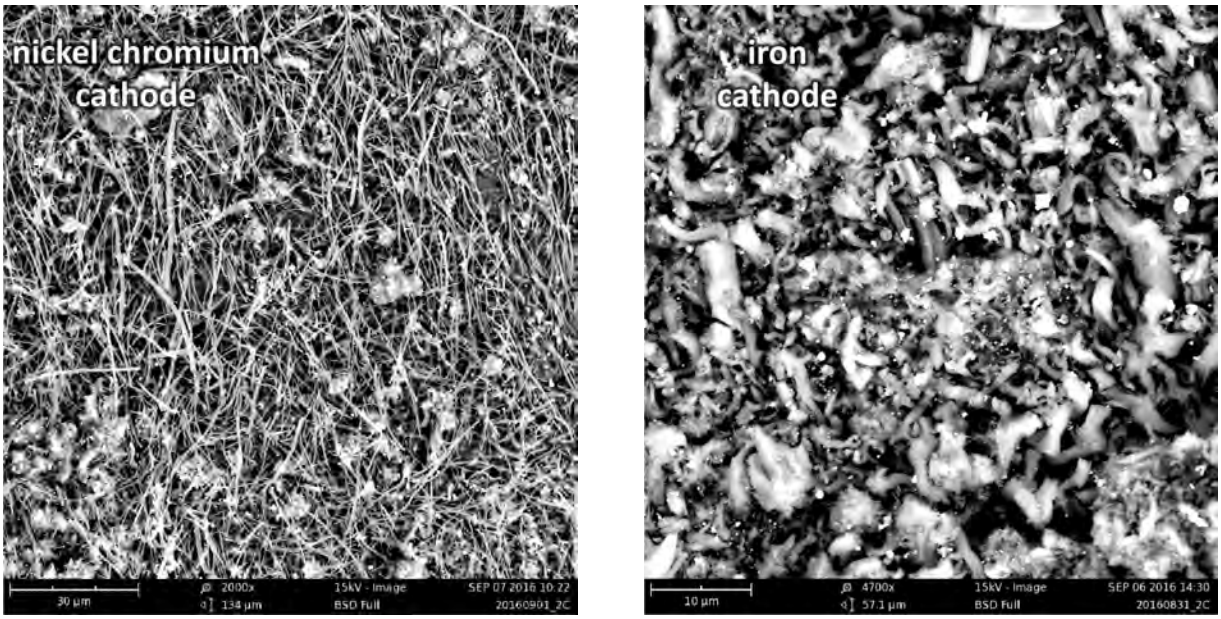

Figure 4. Comparison of the CNT product formed respectively at a nickel chromium alloy (left side) and iron (right side) cathode electrolyses in 770°C Li_2CO_3. The product on Nichrome is formed during intermediate duration (0.8 Ah cm^{-2}), while at an iron cathode, as shown even for short duration electrolysis (0.2 Ah cm^{-2}), the carbon product is highly heterogeneous when formed.

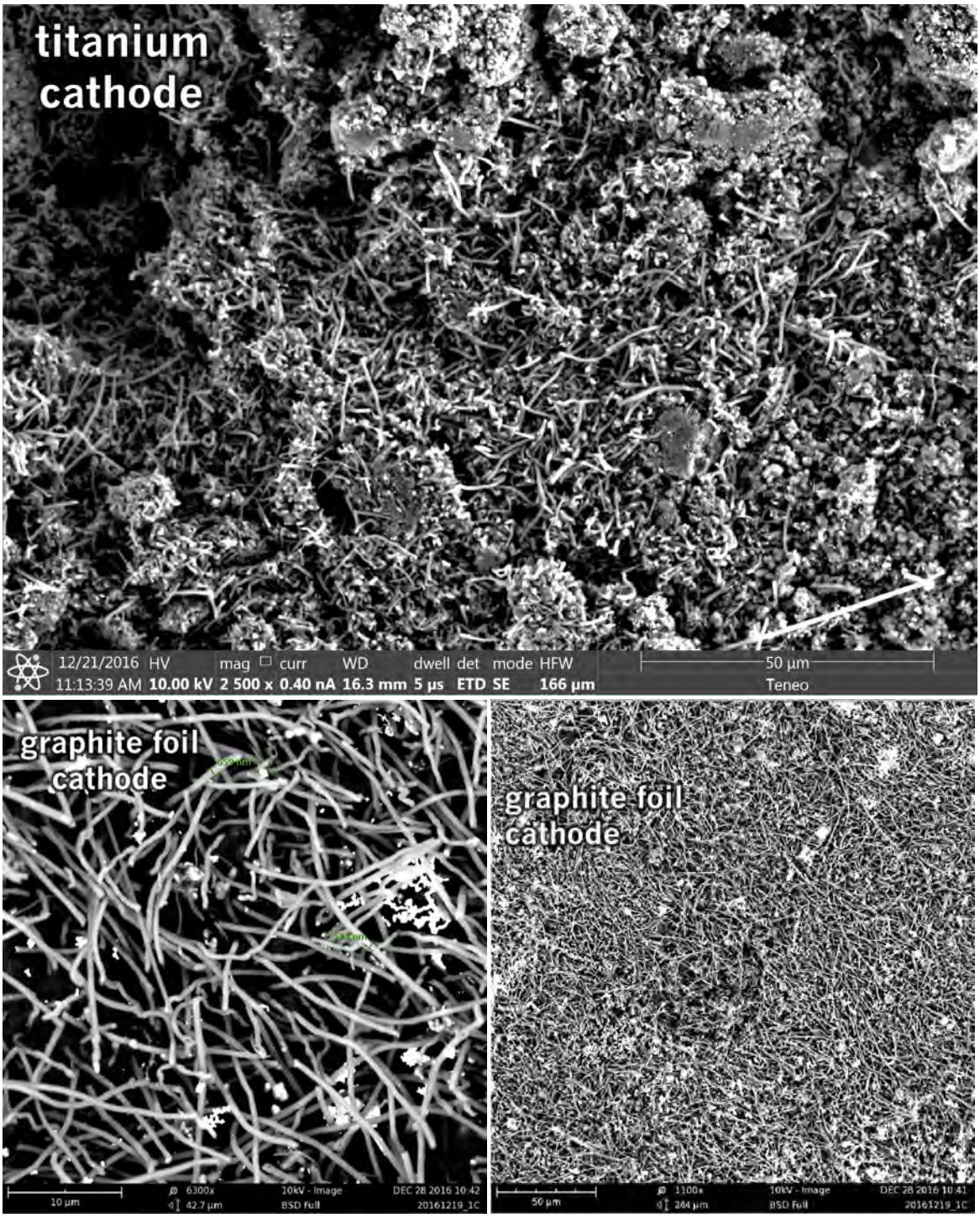

Figure 5. Comparison of the CNT product formed respectively at a titanium (left side) and graphite foil (right side) cathode extended (2.4 Ah cm^{-2}) electrolyses in 770°C Li_2CO_3. The graphite foil is cut as a 5 cm^2 disc, while the titanium (and copper, Monel, iron, steel, nickel or nickel chromium cathode substrate) is coiled wire 5 cm^2 discs.

The physical chemical environment of the conventional CVD CNT synthesis is different than that of the new C2CNT synthesis in most aspects. The latter is an electrochemical process, while the former is chemical. The latter utilizes CO_2, while the former utilizes organics as the reactant, and the latter occurs at the liquid/solid interface, while the latter generally occurs at a gas/solid interface. There are also significant subtle differences. C2CNT provides a higher density of reactive carbon (the molten carbonate electrolyte) near the growth interface, and while an electric field may, or may not, be applied to the substrate during CVD CNT growth, there is always an intense electric field rapidly decreasing through the double layer adjacent to the cathode during C2CNT growth. Despite these differences, it is phenomena that several phenomena here that promote C2CNT processes also appear to have a similar effect on CVD CNT growth processes, and other CVD advances suggest pathways for further C2CNT improvements. Few-layered graphene/multiwalled CNT structures have been observed to form by CVD metal (Ni) substrates (Wang, et al., 2013). In CVD, copper containing substrates can improve carbon mobility that improves the uniformity of the base graphene layer to initiate CNT growth (Zhou 2006). In CVD, larger multiwall CNT (more than ten walled MWCNTs) almost exhibit tip growth with the nucleating metal in the lead, rather than base growth as it is thought be that larger nano-particles adhere less to substrate), while the growth of few walled MWCNTs ($\leq$ 7 walls) are dominated by base growth (Gohiera, 2013). We suggest this is particularly applicable to the new electrochemical C2CNT process as the tip growth also maximizes exposure to the bulk electrolyte and minimizes bulk carbon(IV) diffusion to the growing CNT. In CVD, rapid pre-heating of the catalyst before introduction of the feed gas resulted in the growth of longer/higher yield CNTs, and applied electric field helped promote the growth of more aligned and straighter CNTs (Huang, et al., 2003). In CVD, metal nano-particles can grow and become trapped or move along within the CNT, consuming and requiring more catalyst or stopping the growth process completely (Gozzi, et al., 2006). In single walled CNT CVD growth studies, a nucleation period of 5-10 seconds occurs at the start of the CNT growth. Initially, this nucleation period requires more carbon in proximity to the growth region and less during the next period consisting of a simultaneous CNT growth and repair stage (Qi, et al., 2007). The growth of longer CNTs was facilitated by the initial preparation of micrometer catalyst islands on a substrate CNT (Kong, et al., 1998). Certain pairs of bi-metallic catalysts promote CNT growth 10 to 100 fold better than single metals alone, and splitting the catalyst into two groups, ones that help nucleation more and one that helps growth and repair more leads to the best metal pairs (choose the best from each group), yielding the organization (Wei-Qiao Deng, et al., 2004):

1. (Order of) best: Ni+Co > Ni + Pt >> Cu + Co
   Ni+Co > Ni + Fe ~ Ni >> Fe
   Ni + Co > Ni + Pt > Ni + Cu
2. Nucleation: Co > Pt > Ni slightly less > Cu (poisons)
   Theory: Mo > Cr > Co > Pt > Re > Fe > Ni > Pd
3. Growth & repair: Ni > Co > Pt> Cu
   Theory: Ni + Mo > Ni + Cr > Ni + Co > Ni+ Pt > Ni + Rd > Ni +Fe > Ni > Fe
   & Fe + Mo > Fe + Cr > Fe + Co > Fe + Pt > Fe +Rh > Fe
   & Ni+Mo > Fe + Mo > Co+Mo>Co (2-4 by theory, later Co+Mo > Co

Different metals lead to different diameter CNTs (Zhang, et al., 2008). Islands were found to form on the substrate and their size can lead to optimization (Hofmann, et al., 2007).

II. C2CNT intermediate length CNTs with intermediate integrated electrolysis charge transfer:

Figure 6 presents an intermediate stage of the C2CNT synthesis advancement resulting in improved CNT yield and improved CNT length. In this intermediate advancement of synthesis, a bare Monel (rather than galvanized steel) substrate was used, a 2-step (0.05 A/13 min, 0.25 A/12min), rather than the original 4-step electrolysis pre-activation was utilized, and 0.4 g (0.8 wt%) of Ni powder was added to the 50 g of 770°C Li_2CO_3. electrolyte, and an Ir anode, and a somewhat higher current density and integrated charge was used was used (1 A through the 5 cm^2 electrode (0.2 A cm^{-2}), for 6 hours (integrated charge of 1.2 Ah cm^{-2}). The higher constant current resulted in a higher (1.6 V) potential during the electrolysis. Up to 10 wt% added $LiBO_2$ was observed to have no effect on the observed CNT morphology, but as described in section 1 enhances their electrical conductivity. The electrolysis product shown in Figure 6 contains 3 g $LiBO_2$ added to the electrolyte. As seen in the figure, even without the additional improvements of mixed Ni/Cr, rather than just Ni, nucleation, and without electrolyte aging, the CNT quality is high and the tangled CNTs are longer, ranging from 20 to over 200 µm in length.

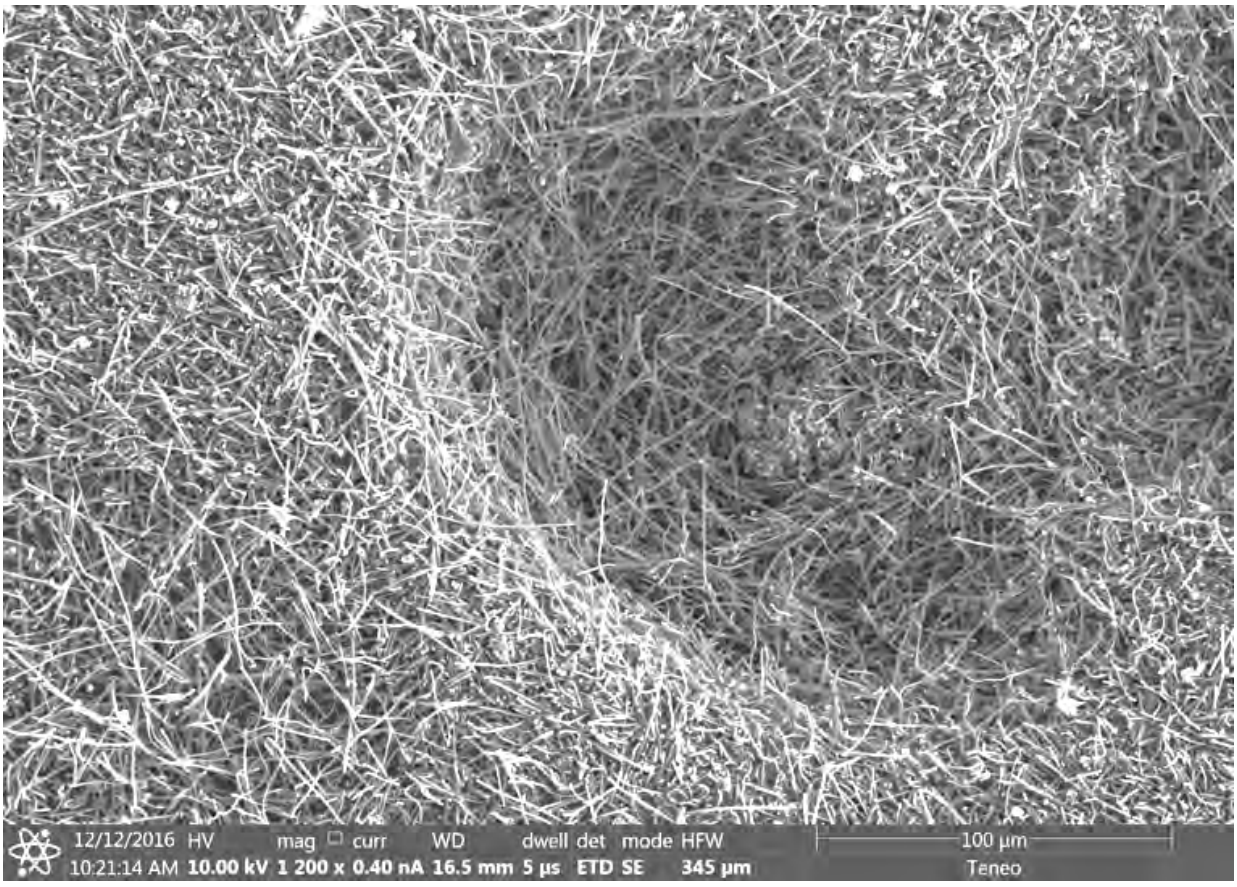

Figure 6. SEM of B-doped CNTs formed by 6 Ah electrolysis at a 5 cm^2 Monel cathode in 5g $LiBO_2$ and 50 g Li_2CO_3 at 770°C.

III. C2CNT admixing of sulfur, nitrogen and phosphorous (in addition to boron, section I) to carbon nanotubes:

Here, we show the first single step electrosynthesis of sulfur heteroatom CNTs. Sulfur doped carbons, including CVD grown CNTs, have a variety of applications (Kicinski, 2014; Cui, 2011). Unlike in pure carbonate (Ren, et al., 2017), previously no carbon product (CNT or otherwise) was observed to form at the cathode during the electrolysis of 1 mol % (or 3, or 5 mol %) Li_2SO_4 in 770°C Li_2CO_3. The observed potentials at 1 A are lower with higher [Li_2SO_4] (and are lower than the 1-2 volt electrolysis potential observed without Li_2SO_4). This lack of CNT formation is in accord with the electronegativity of sulfur compared to carbon, which favors the thermodynamic formation of the former compared to the latter. To improve the energetics of carbon formation, the concentration of sulfate is decreased (relative to carbonate) creating a pathway to the observed formation of sulfur containing CNTs. Specifically, the Figure 7's left side presents sulfur containing CNTs from molten carbonate electrolysis with 0.1 mole% sulfate subsequent to a 2-hour electrolysis at 1 A (using the conventional galvanized steel cathode and Ni 200 wire anode and without added Ni metal powder). EDS of the CNT product measured 0.1 mole % of sulfur in the CNT product. As in previous experiments, prior to this higher current extended electrolysis, cathode nucleation was facilitated by an application of lower constant currents sequentially applied (each for 10 minutes) and increased from 0.05, 0.10, 0.25 to 0.5 A. As previously observed with successful (non-sulfur containing electrolyte) CNT electrolyses (Ren, et al., 2015; Ren, et al., 2017; Ren and Licht, 2016; Wu, 2016), the initial 10-minutes lowest current electrolysis occurred at a potential of 0.4 to 0.5 V, which is consistent with the expected nucleation by Ni on the cathode while each of the subsequent increasing constant currents occurred at increasing potentials between 1 to 2 V.

The previous electrolytic formation of P-heteroatom CNTs from lithium metaphosphate dissolved in a lithium carbonate electrolyte (Ren, et al., 2017) is improved here, including the first evidence of phosphorous in the CNT product. The use of $LiPO_3$ is observed to facilitate salt dissolution in the lithium carbonate electrolyte. Variations which led to the improved length and yield of P-containing CNTs include an increase from the previous 1 % to 5 mol % $LiPO_3$**,** and the use of a Monel, rather than galvanized steel cathode. On the right side of Figure 7, the product P-heteratom long (300-600 μm) are produced with intermediate 0.8 Ah cm^{-2} charge at a low current density of 0.03 A cm^{-2}; a conventional (Ni 200) anode and no Ni powder was added to the electrolyte during this C2CNT synthesis, EDS of the CNT product measured 0.3 mole % of phosphorous in the CNT product. This is substantially lower than the electrolytic concentration of phosphorous, and the P-heteroatom may provide a poor lattice match to the CNT.

As with boron, sulfur and nitrogen doping, nitrogen doping of CNTs can lead to a variety of specialized applications (Ren, et al., 2017). An N-CNT product is also observed from electrolysis of $LiNO_3$ in the 770°C Li_2CO_3 electrolyte. In this case, the yield of CNTs improves with a 5 mole %, compared to a 1 mole %, dissolution of $LiNO_3$ within the electrolyte. Presumably, the added, dissolved lithium nitrate equilibrates to lithium nitrite in the molten electrolyte, analogous to the known solid state thermal decomposition:

solid $LiNO_3$ thermal decomposition occurs above 500°C: $LiNO_3 \rightarrow LiNO_2 + 1/2O_2$ (1)

Subsequent to electrolysis, EDS analysis of nitrogen within the product is indicated, but not confirmed, as the EDS instrumentation was broad and not capable or resolving the near lying carbon (12.01) and nitrogen (14.01) peaks. SEM and an extended analysis of the nitrogen CNT product, and also a detailed analysis of the doped CNT growth mechanism, further elemental probes of each of the heteroatom modified CNTs, and applications of these CNTs will each be presented in an expanded, future investigation.

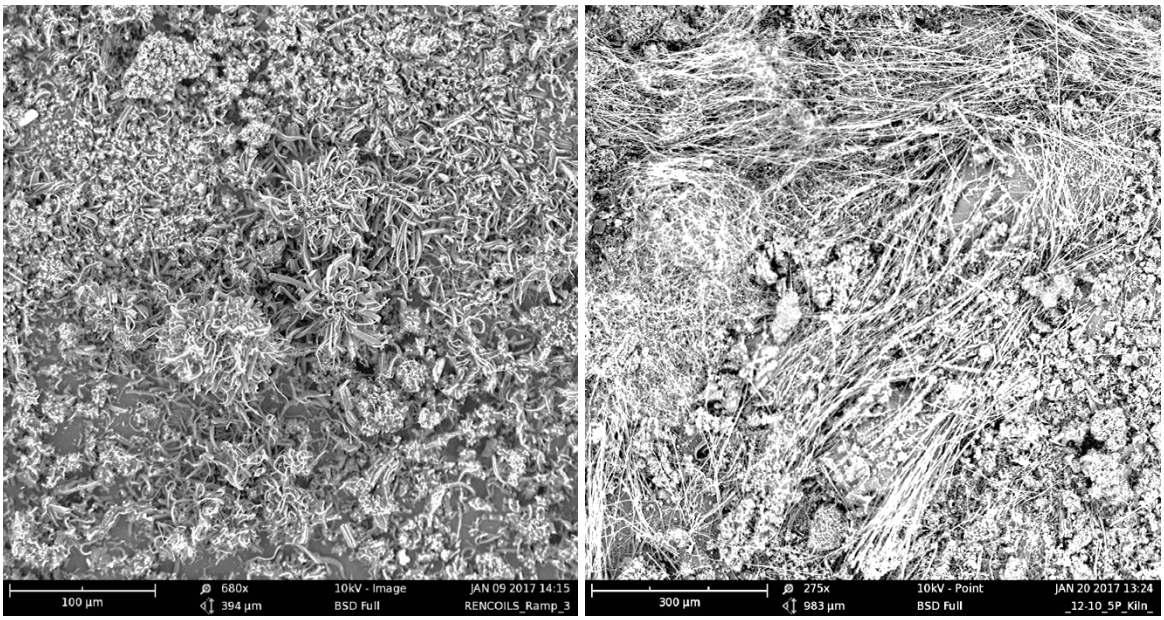

Figure 7. Left: SEM of the S-heteroatom product formed by 0.4 Ah cm^{-2} electrolyis at a galvanized steel cathode in 50g of 770°C Li_2CO_3 containing 0.074g Li_2SO_4. Right: SEM of the P-heteroatom product formed by 0.8 Ah cm^{-2} electrolyis at a Monel cathode in 50g of 770°C Li_2CO_3 containing 0.5 mol % Li_2PO_4.

The electrosynthesis of CNTs containing the heteroatoms of sulfur, phosphorus or boron, and likely nitrogen, is observed. Doped CNTs can have unusual, useful properties including high electrical conductivity, ctalysis, heavy metal removal, enhanced oxygen kinetics and improved charge storage**.**

IV. Scalability & cost of the C2CNT process:

As an electrochemical process, C2CNT is linearly scale-able with our increasing area of the electrolysis chamber (Licht, 2017), Figure 8.

Figure 8. The evolution of the electrolysis chamber. Earlier versions can be seen in the front on the left, and later versions in the back and to the right. The rectangular electrolysis chambers use the interior walls as the air electrode (Licht, 2017).

The thermodynamic and cost savings of new and retrofit gas, cement, and coal power plants has been analyzed (Lau, et al., 2016; Licht, 2017). Industrial plant retrofit provides a ready source of hot CO_2 for electrolysis, and the added the oxy-fuel energy benefits (in addition to the benefit of CO_2 removal and the production of CNTs) of the C2CNT co-product O_2 looped back into the plant, the value of the CNT product is illustrated in Figure 9. The top of the figure shows this oxy-fuel advantage with a gas combined cycle power plant. The bottom right and left of the figures show this oxy-fuel advantage respectively, in cement or coal power or cement plants. In the lower portion of the figure, the electrical power for the electrolysis C2CNT component is provide by renewable energy (solar or wind power, respectively), as opposed to utilizing electricity from the fossil fuel (gas) power plant. It should be noted that conventional deleterious coal plant sulfur and nitrogen emissions might instead be beneficial, when considered as a source of CNT heteroatom doping as descried in Section III. Such gas, coal and cement plants provide further impetus for substantial intermediate C2CNT scale-up en route to direct atmospheric transformation of CO_2 to CNTs.

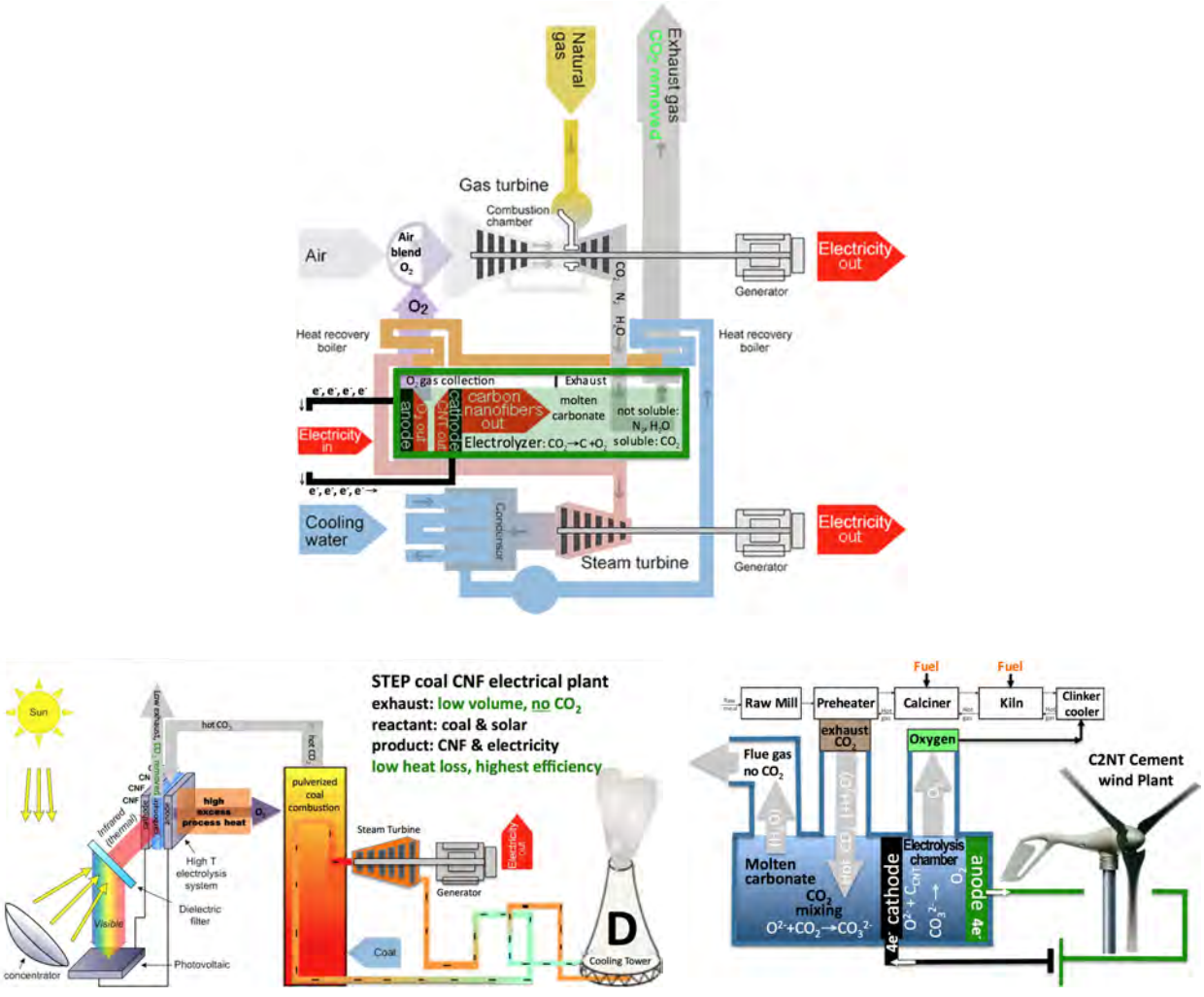

Figure 9. Top: Schematic of a CNT combined cycle power plant (Lau, et al., 2016). Middle: Transforming CO_2 emissions from a coal combustion plant into CNTs using solar energy (Lau, et al., 2016). Bottom: C2CNT Cement wind plant: The full oxy-fuel configuration is shown. The plant does not emit CO_2, and over time cement produced absorbs CO_2. Hence the process is carbon negative, which compares favorably to the large positive carbon signature of conventional cement plants (Licht, 2017).

Cost analysis here is structured on eliminating (by transformation to CNTs) the CO_2 exhaust from a gas, coal or cement plant (Lau, 2016 and Licht 2017). The cost incorporates the increased fuel combustion efficiency in these plants when the C2CNT oxygen product ($CO_2 \rightarrow$ CNT + O_2) is looped back into the plant's fuel combustion (Zheng, 2011).

This analysis is derived from a comparison to the known cost structure of a comparable, mature industry: aluminum production. The C2CNT process bears many similarities to aluminum smelting. Both processes consist of molten electrolysis, and do not use noble or exotic materials. Aluminum smelting produces aluminum metal from alumina (using bauxite, sodium hydroxide and electricity), while C2CNT produces carbon nanotubes from carbon dioxide (using carbon dioxide and electricity). Aluminum smelting operates at 960°C in a molten cryolite electrolyte. The C2CNT process operates under somewhat milder conditions at 770°C in a less exotic, molten carbonate electrolyte. Both processes operate at high rate (hundreds of mA per cm^2) and low polarization. In both cases the electrolysis chamber consists of common metals, common insulators (such as kiln or "firebricks"), and control equipment. Electrolysis in the Aluminum smelting process is driven at approximately 4 volts using 3 electrons per aluminum. The C2CNT electrolysis is driven at approximately 1 volt using 4 electrons per carbon dioxide. C2CNT and aluminum smelters have approximately equivalent output (tonnage) rates.

Aluminum costs ~$1,880 per metric ton, of which ~32% of the cost is electricity (Djukanovic, 2012). Today's newer, more efficient Al plants require 12 MWh per ton, whereas older Al plant require 15 MWh per ton. 13 MWh is measured and calculated from a 94% efficient 3 electron per Al electrolysis at 4.1V (Naixiang, 2014). $600 for 12 MWh = $0.05 per kWh. This Al electricity cost varies from lowest (in the Middle East) at $300, to mid range $650 (US), to highest (China with high energy tariffs) of $1,020/ton.

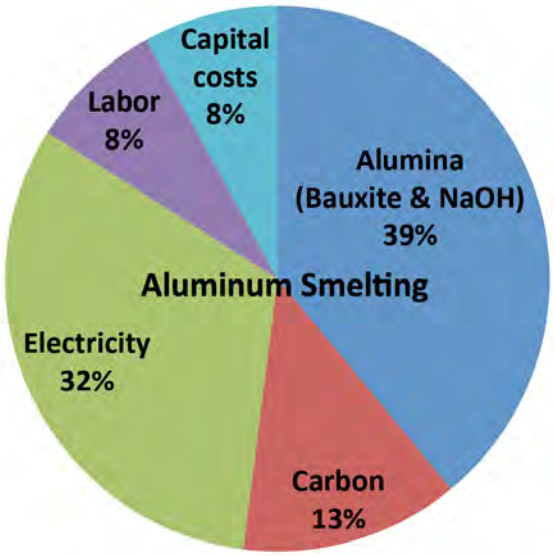

Figure 10. Aluminum smelter cost structure (modified from Djukanovic, 2012).

A breakdown of Al production costs per metric ton (tonne) of Al, based on market costs are summarized in Figure 10 and Table 1, and consists of: Consumable Expenses (32% electricity & 52%; reactants = 84%), Electricity: 32%, Labor: 8%, and Capital Expenses (amortized cost of electrolyzers, processing equipment, and miscellaneous overhead). Note that the energy to drive the aluminum production originates from two sources (electricity and energy released from the consumed carbon anode).

Table 1. Comparison of aluminum and C2CNT production costs.

Process	$US Cost (% of total)					
	alumina	carbon	electricity	labor	capital	total
Aluminum	733(39%)	$244(13%)	$602(32%)	$150 (8%)	$150 (8%)	$1880(100%)
	CO_2	-	electricity	labor	capital	total
C2CNT	$0	$0	$360	$150	$150	$660

As compared in Table 1, and unlike Al smelting, the C2CNT process uses a no-cost oxide as the reactant (carbon dioxide, rather than bauxite). Both are straightforward, high current density electrochemical (molten electrolytic reduction of oxide) processes. The C2CNT process operates under somewhat milder conditions at 770°C in a less exotic, molten carbonate electrolyte at similar rates of output, and to a first order of approximation, both processes will be assumed to have the same labor and capital costs. Whereas, Al production requires ~13 MWh per ton of aluminum, C2CNT production requires less energy (7 MWh) per ton of carbon nanotubes. This energy is calculated here from the C2CNT 1 volt electrolysis consuming 4 electron per carbon dioxide splitting efficiency. The observed electrolysis voltage varies from 0.8V to up to 2V, decreasing with higher concentrations of added lithium oxide, and increasing with current density and with mixed molten carbonate electrolytes (Ren, 2015; Ren, 2017). Using the formula weight to convert mass carbon dioxide to moles, and Faradays constant at 1V yields 2.4 MWh

per ton CO_2, which decreases to 2.0 MWh per ton CO2 (which is 7.2 MWh per CNT) by the 20% energy recovered through driving the turbine more efficiently with pure oxygen (looped in from the C2CNT electrolysis), rather than regular air, combustion (Lau, 2016). This yields an electrical cost of $360 per ton CNT, and as summarized in Table 1, a total cost of $660 per ton of CNT. The electrical cost falls per ton CNT based on less expensive wind electric, equivalent to (x12.01/44.01) $50 per ton of CO_2 (Licht, 2017). Higher production rates will increase this cost, while the imposition of a carbon tax or carbon credits will lower this cost.

C2CNT atmospheric mitigation does not require pre-concentration of the CO_2. Heat is then provided using photovoltaic discarded thermal sunlight (Li, et al., 2011) as illustrated in Figure 11.

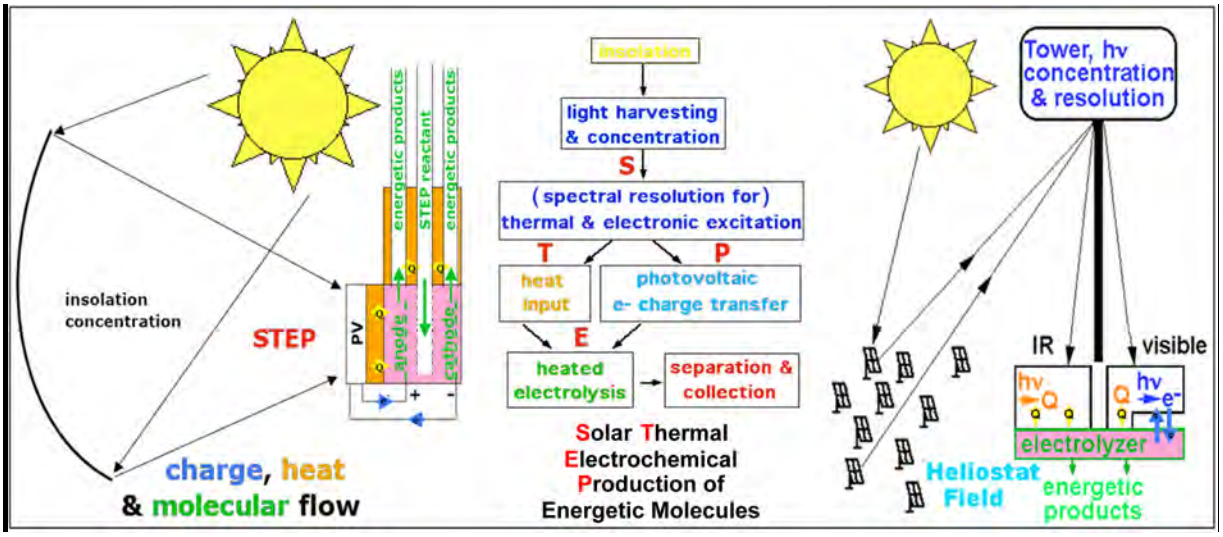

Figure 11. Global use of sunlight to drive the formation of energy rich molecules. Left: Charge, & heat flow in STEP: heat flow (yellow arrows), electron flow (blue), and reagent flow (green). Right: Beam splitters redirect sub-bandgap sunlight away from the PV onto the electrolyzer (Licht, et al., 2011).

The following section is expanded by addition of a CO_2 availability concluding paragraph from "Scalability of STEP Processes" section of (Licht, 2011), which in turn was expanded from the text and Supporting Information from (Licht, et al., 2010). Note, since this 2011 analysis, subsequent total estimates of the extent of CO_2 released in industrial revolution have increased to over 1.1 teratons.

STEP can be used to remove and convert CO_2. As with water splitting, the electrolysis potential required for CO_2 to CO splitting falls rapidly with increasing temperature, and we have shown that a photovoltaic, converting solar to electronic energy at 37% efficiency and 2.7V, may be used to drive three CO_2 splitting, lithium carbonate electrolysis cells, each operating at 0.9V, and each generating a 2 electron CO product. The energy of the CO product is 1.3V (eq 1), even though generated by electrolysis at only 0.9V due to synergistic use of solar thermal energy. At lower temperature (770°C, rather than 950°C), carbon, rather than CO, is the preferred product, and this 4 electron reduction approaches 100% Faradaic efficiency.

The CO_2 STEP process consists of solar driven and solar thermal assisted CO_2 electrolysis. Industrial environments provide opportunities to further enhance efficiencies; for example fossil-fueled burner exhaust provides a source of relatively concentrated, hot CO_2. The product carbon may be stored or used. STEP represents a new solar energy conversion processes to produce energetic molecules. Individual components used in the process are rapidly maturing technologies including wind electric, molten carbonate fuel cells, and solar thermal technologies.

It is of interest whether material resources are sufficient to expand the process to substantially impact (decrease) atmospheric levels of CO_2. The buildup of atmospheric CO_2 levels from a 280 to 392 ppm occurring over the industrial revolution comprises an increase of 1.9×10^{16} mole (8.2×10^{11} metric tons) of CO_2, and will take a comparable effort to remove. It would be preferable if this effort produces useable, rather than sequestered, resources. We calculate below a scaled-up STEP capture process can remove and convert all excess atmospheric CO_2 to carbon.

In STEP, 6 kWh m^{-2} of sunlight per day, at 500 suns on 1 m^2 of 38% efficient CPV, will generate 420 kAh at 2.7 V to drive three series connected molten carbonate electrolysis cells to CO, or two series connected series connected molten carbonate electrolysis cells to form solid carbon. This will capture 7.8×10^3 moles of CO_2 day^{-1} to form solid carbon (based on 420 kAh · 2 series cells / 4 Faraday mol^{-1} CO_2). The CO_2 consumed per day is three fold higher to form the CO product (based on 3 series cells and 2 F mol^{-1} CO_2) in lieu of solid carbon. The material resources to decrease atmospheric CO_2 concentrations with STEP carbon capture, appear to be reasonable. From the daily conversion rate of 7.8×10^3 moles of CO_2 per square meter of CPV, the capture process, scaled to 700 km^2 of CPV operating for 10 years can remove and convert all the increase of 1.9×10^{16} mole of atmospheric CO_2 to solid carbon. A larger current density at the electrolysis electrodes, will increase the required voltage and would increase the required area of CPVs. While the STEP product (chemicals, rather than electricity) is different than contemporary concentrated solar power (CSP) systems, components including a tracker for effective solar concentration are similar (although an electrochemical reactor, replaces the mechanical turbine). A variety of CSP installations, which include molten salt heat storage, are being commercialized, and costs are decreasing. STEP provides higher solar energy conversion efficiencies than CSP, and secondary losses can be lower (for example, there are no grid-related transmission losses). Contemporary concentrators, such as based on plastic Fresnel or flat mirror technologies, are relatively inexpensive, but may become a growing fraction of cost as concentration increases. A greater degree of solar concentration, for example 2000 suns, rather than 500 suns, will proportionally decrease the quantity of required CPV to 175 km^2, while the concentrator area will remain the same at 350,000 km^2, equivalent to 4% of the area of the Sahara Desert (which averages ~6 kWh m^{-2} of sunlight per day), to remove anthropogenic CO_2 in ten years.

700 km^2 of CPV plant will generate 5×10^{13} A of electrolysis current, and require ~2 million metric tonnes of lithium carbonate, as calculated from a 2 kg/liter density of lithium carbonate, and assuming that improved, rather than flat, morphology electrodes will operate at 5 A/cm^2 (1,000 km^2) in a cell of 1 mm thick. Thicker, or lower current density, cells will require proportionally more lithium carbonate. Fifty, rather than ten, years to return the atmosphere to pre-industrial CO_2 levels will require proportionally less lithium carbonate. These values are viable within the current production of lithium carbonate. Lithium carbonate availability as a global resource has been under recent scrutiny to meet the growing lithium battery market. It has been estimated that the current global annual production of

0.13 million metric tons of LCE (lithium carbonate equivalents) will increase to 0.24 million tons by 2015. Alternative, mixed alkali/alkali earth carbonates are also suitable. Sodium carbonate is substantially more available, and as noted can be combined with lithium carbonate for molten CO_2 splitting. Low velocity natural wind speeds are sufficient to move this air to C2CNT processors. A 100 km by 100 km area with wind moving through it at 2 km per hour will deliver over a teraton of CO_2 during a decade.

Acknowledgements

We are grateful to the Unites States National Science Foundation grant 1505830 for partial support of this Data Article.

References

Cui, T., Lv, R., Huang, Z., Kang, F. and Wu, D. (2011). Effect of sulfur on enhancing nitrogen-doping and magnetic properties of carbon nanotubes. Nanoscale Res. Lett. 6, 27191-27196.

Dey, G., Ren, J., El-Ghazawi, T., and Licht, S. (2016). How does an amalgamated Ni cathode affect carbon nanotube growth? A density functional theory study. RSC Adv. 6, 27191-27196.

Djukanovic, (2012) Analysis of production costs in the aluminum smelting industry. Aluminum 7-8, 28-32.

Gohiera, A., Ewelsa, C. P., Mineab, T.M., and Djouadia, M.A. (2008). Carbon nanotube growth mechanism switches from tip- to base-growth with decreasing catalyst particle size. Carbon 46, 1331-1338.

Gozzi, D., Latini, A., Capannelli, G., Canepa, F., Napoletano, M., Cimberle, M.R., and Tropeano, M. (2006). Synthesis and magnetic characterization of Ni nanoparticles and Ni nanoparticles in multiwalled carbon nanotubes. J. Alloys Composites 419, 32–39.

Hofmann, S., Sharma, R., Ducati, C., Du, G, Mattevi, C., Cepek, C., Cantoro, M., Pisana, S., and Parvez, A. (2007). In situ Observations of Catalyst Dynamics during Surface-Bound Carbon Nanotube Nucleation. Nano Lett. 7, 602-608.

Huang, S., Cai, X., and Liu, J. (2003). Growth of Millimeter-Long and Horizontally Aligned Single-Walled Carbon Nanotubes on Flat Substrates. J. Amer. Chem. Soc. 125, 5636-5637.

Kicinski, W., Szala, M., Bystrzejewski, M. (2014). Growth of Millimeter-Long and Horizontally Aligned Single-Walled Carbon Nanotubes on Flat Substrates. Carbon 68, 1-32.

Johnson, M., Ren, J., Lefler, Licht, G., Vicini, J., Liu, X., Licht, S. Carbon Nanotube Wools Made Directly from CO_2 by Molten Electrolysis: Value Driven Pathways to Carbon Dioxide Greenhouse Gas Mitigation. Materials Today Energy, in press.

Kong, J., Soh, H. T., Cassell, A. M., Quate, C. F., and Dai, H. (1998). Synthesis of individual single-walled carbon nanotubes on patterned silicon wafers. Nature 395, 878-881.

Lau, J., Dey, G., and Licht., S. (2016). Thermodynamic assessment of CO_2 to carbon nanofiber transformation for carbon sequestration in a combined cycle gas or a coal power plant. Energy Conservation and Management, 122, 400-410.

Licht. S., Wang, B., Ghosh, S., Ayub, H. Jiang, D., and Ganley, T. (2010). A New Solar Carbon Capture Process: STEP Carbon Capture. J. Phys. Chem. Lett. 1, 2363-2368.

Licht. S. (2011). Efficient Solar-Driven Synthesis, Carbon Capture, and Desalinization, STEP: Solar Thermal Electrochemical Production of Fuels, Metals, Bleach. Adv. Mat. 23, 5592-5612.

Licht, S., Douglas, A., Ren, J., Carter, R., Lefler, M., and Pint, C. L. (2016). Carbon Nanotubes Produced from Ambient Carbon Dioxide for Environmentally Sustainable Lithium-Ion and Sodium-Ion Battery Anodes. ACS Central Science, 2, 162-168.

Licht, S. (2017). Co-Production of Cement and Carbon Nanotubes with a Carbon Negative Footprint. J. CO2 Utilization, 18, 378-389.

Naixiang, F., Jianping, P., Qengren, N., Lei, Z., Ning, K., Xian, L., Xiaofeng, G., Towards decreasing energy consumption of aluminum reduction, Light Metals 2014, 517-520.

Ren, J., Li, F., Lau, J., Gonzalez-Urbina, L., and Licht, S. (2015). One-pot synthesis of carbon nanofibers from CO_2. Nano Lett. 15, 6142-6148.

Ren, J., Lau, J., Lefler, M., and Licht, S. (2015). The Minimum Electrolytic Energy Needed to Convert Carbon Dioxide to Carbon by Electrolysis in Carbonate Melts. J. Phys. Chem. C 119, 23342-23349.

Ren, J., Johnson, M., Singhal, R., and Licht, S. (2017). Transformation of the greenhouse gas CO_2 by molten electrolysis into a wide controlled selection of carbon nanotubes. J. CO2 Utilization 18, 335-344.

Qi, H., Yuan, D., and Liu, J. (2007). Two-Stage Growth of Single-Walled Carbon Nanotubes. J. Phys. Chem. C 111, 6158-6180.

Wang, W., Guo, S., Penchev, M., Ruiz, I., Krassimir, K., Bozhilov, N., Yan, D., Ozkan, M., and Ozkan, C.S. (2013). Three dimensional few layer graphene and carbon nanotube architechures for high fidelity supercapacitors. Nano Energy, 2, 294-303.

Wei-Qiao Deng, D., Xu, X., and Goddard, W. A. (2004). A Two-Stage Mechanism of Bimetallic Catalyzed Growth of Single-Walled Carbon Nanotubes. Nano Lett. 4, 2331-2335.

Zhang, Y., Zhou, W., Jin, Z., Ding, Li., Zhang, Z., Liang, X., and Li, Y. (2008). Direct Growth of Single-Walled Carbon Nanotubes without Metallic Residues by Using Lead as a Catalyst. Chem. Mater., 20, 7521–7525.

Zheng L. (2011). Oxy-fuel combustion for power generation and carbon dioxide (CO2) capture. Woodhead Publishing; ISBN 9781845696719; 400 p.

Zhou, W., Han, Z., Wang, J., Zhang, Y., Jin, Z., Sun, X., Zhang, Y., Yan, C., and Li, Y., (2006). Copper Catalyzing Growth of Single-Walled Carbon Nanotubes on Substrates. Nano Lett. 6, 2987-2990.